Murphy, R.M.; Richards, K.G.; Krol, D.J.; Gebremichael, A.W.; Lopez-Sangil, L.; Rambaud, J.; Cowan, N.; Lanigan, G.J.; Saunders, M.. 2022. **Assessing nitrous oxide emissions in time and space with minimal uncertainty using static chambers and eddy covariance from a temperate grassland.**

The definitive version was published in *Agricultural and Forest Meteorology*, 313, 108743. 14, pp. https://doi.org/10.1016

The definitive version is available at https://www.elsevier.com/

Assessing nitrous oxide emissions in time and space with minimal uncertainty using static chambers and eddy covariance from a temperate grassland

Murphy, R.M. [1,2] Richards, K.G.[2] Krol, D. [2] Gebremichael, A, [2] Lopez-Sangil, L. [2] Rambaud, J. [2] Cowan, N.[3] Lanigan G.J.[2] and Saunders, M.[1]

[1]Department of Botany, Trinity College Dublin, Dublin 2, Ireland

[2]Teagasc Johnstown Castle, Wexford, Ireland

[3]UK Centre for Ecology and Hydrology, Bush Estate, Penicuik, Midlothian, UK.

Corresponding author: Rachael Murphy (murphr32@tcd.ie)

Keywords:

Methodology, Nitrous oxide, Agriculture, Grassland, Uncertainty

ABSTRACT

Where nitrogen input from fertilizer application exceeds plant demands, hotspots of microbially produced nitrous oxide (N_2O) can exhibit disproportionately high rates of emissions relative to longer periods of time, known as hot moments. Hotspots and hot moments of N_2O are sensitive to changes in agricultural management and weather, making it difficult to accurately quantify N_2O emissions. This study investigates the spatial and temporal variability of N_2O emissions using both static chambers (CH) and eddy covariance (EC) techniques, measured at a grassland site subject to four fertilizer applications of calcium ammonium nitrate (CAN) in 2019. Daily mean CH emissions were calculated using the arithmetic method and Bayesian statistics to explicitly account for the log-normal distribution of the dataset. N_2O fluxes measured by CH and EC were most comparable when flux measurements were > 115 N_2O-N µg m^{-2} hr^{-1}, and EC and CH measurements showed spatial and temporal alignment when CH n ≥ 15. Where n ≤ 5, the Bayesian method produced large uncertainties due to the difficulty of fitting an arithmetic mean from a log-normally distributed data set with few flux measurements. Annual EC fluxes, gap-filled using a multi-variate linear model, showed a strong correlation with measured flux values ($R^2 = 0.92$). Annual cumulative fluxes by EC were higher (3.35 [± 0.5] kg N ha^{-1}) than CH using the arithmetic (2.98 [± 0.17] kg N ha^{-1}) and Bayesian method (3.13 [± 0.24] kg N ha^{-1}), which quantified emission factors of 1.46%, 1.30% and 1.36%, respectively. This study implies that a large sample size and frequent CH flux measurements are necessary for comparison with EC fluxes and that Bayesian statistics are an appropriate method for estimating realistic means and ranges of uncertainty for CH flux data sets.

INTRODUCTION:

Nitrous oxide (N_2O) is a powerful greenhouse gas (GHG), with a global warming potential (GWP) 265 times that of carbon dioxide (CO_2), and a lifespan of over 100 years (IPCC, 2013) The global average concentration of atmospheric N_2O reached 331.1 ± 0.1 ppb in 2018, 23% greater than pre-industrial levels (270 ppb) and is primarily associated with the application of mineral or organic nitrogen (N) to soils (WMO, 2019). Nitrogen fertilizers provide mineral N in the form of ammonium (NH_4^+) and nitrate (NO_3^-) for the purpose of growing crops; however, soil microbes also consume this N to produce N_2O through the processes of nitrification and denitrification (Luo *et al.* 2017). Where N is applied to soil when conditions favour these microbial processes (water filled pore space (WFPS) 70 – 80%, (Linn and Doran, 1984), substrate availability [nitrate (NO_3^-) and ammonium (NH_4^+)] (Zanatta *et al.* 2010), temperature induced increases in soil respiration (Butterbach-Bahl *et al.* 2013)), hotspots of N_2O can occur, releasing short-lived, but excessively high rates of emissions (Hargreaves *et al.* 2015). Hotspots coincide with changes in substrate availability, resources or the physical environment (Pickett and White, 1985) for example, dry-wetting cycles of soils or increases in soil moisture following fertilizer application where soil conditions become favourable for microbial N_2O production (Fuchs *et al.* 2018). Pulses of N_2O from hotspots can exhibit rates of emissions that are 15-30% higher relative to longer periods of time. These emission events are known as hot moments (McClain *et al.* 2003), and typically last between 5-20 days (Groffman *et al.* 2009).The occurrence of N_2O hotspots and hot moments result in extremely heterogeneous emissions across agricultural landscapes (Cowan *et al.* 2017) and it is extremely difficult to accurately quantify N_2O emissions without large uncertainties.

Micrometeorological techniques such as eddy covariance (EC) have been extensively used to quantify fluxes of CO_2 and methane (CH_4) between the soil and the atmosphere within grassland ecosystems (Felber *et al.* 2015; Soussana *et al.* 2010). One main advantage of EC techniques is that it continuously measures the ecosystem to atmosphere exchange of key gas scalars that are integrated at the ecosystem scale without disturbing the soil or altering the microclimate (Wang *et al.* 2013). However, due to the lower atmospheric concentrations of N_2O and the higher sensitivities needed to capture baseline emissions (relative to CO_2), it is only in more recent years that the EC technique has been capable of reliably measuring field-scale N_2O fluxes through the development and deployment of fast, high precision absorption spectrometers such as quantum cascade lasers (QCL) (Voglmeier *et al.* 2019). In contrast, static chambers (CH) measurements are the most commonly used method for quantifying field fluxes of N_2O (Bell *et al*. 2016; Maire *et al.* 2020; Rochette, 2011). Manually-operated CH are relatively inexpensive to run, easy to deploy, have well-established standardised guidelines for GHG measurements and are a highly cited method for investigating N fertilization effects on soil N_2O fluxes (de Klein *et al.* 2015;Krol *et al*. 2017; Maire *et al*. 2020). However, CH flux measurements provide lower spatial and temporal resolution when compared to EC techniques, as single measurements are typically made at a daily time-step over an area less than 1 m^2. Therefore, peak emissions, diurnal variation and decay patterns of N_2O over time following rainfall or re-wetting of dry soils and/or management interventions such as fertilizer application, are not always fully captured using CH methods (Jones *et al.* 2011). The peak and decay pattern which is commonly observed in CH N_2O fluxes over time, typically display a log-normal distribution in space which is characterized by a small number of high flux values (Levy *et al.* 2017). The probability density of a log-normally distributed N_2O flux ($Flux_{N_2O}$) at a given time is Eq. (1):

$$f\left(Flux_{N_2O}\right) = \frac{1}{\sqrt{2\pi}\sigma_{log}\, Flux_{N_2O}} e^{-(\log\left(Flux_{N_2O}\right)-\mu_{log})^2/2\sigma_{log}^2}$$

where μ_{log} and σ_{log} are the mean and standard deviation of the log-transformed flux. The mean distribution without log transformation is given by Eq (2):

$$\mu = \exp(\mu_{log} + 0.5\ \sigma_{log}^2)$$

Quantifications of the variables which make up the log-normal distribution, μ_{log} and σ_{log} (and therefore the true μ) are often insufficient because of the large variability, measurement error and small sample size (Levy *et al.* 2017). In order to improve estimates of CH flux measurements and make localized field measurements more comparable with ecosystem scale EC flux measurements over space and time, a method is required, that accounts for the uncertainty in μ which arises from estimating field-scale fluxes from a small, log-normally distributed sample. More recently, Bayesian statistics have been utilized to analyse N_2O fluxes as a lognormal distribution and in doing so, reduce the spatiotemporal uncertainty associated with CH flux measurements (Cowan *et al*. 2020; Nishina *et al*. 2009)

The objective of this paper was to investigate both technical disparities (spatially and temporally) between EC and CH in measuring N_2O fluxes, as well as the methods used to handling CH N_2O flux data (arithmetic and Bayesian) for a complete comparison between methodologies. In this study we aim to (i) address the uncertainty in upscaling CH N_2O flux measurements to the field scale by using a Bayesian approach to account for the log-normal distribution of flux measurements and to provide realistic means (ii) compare N_2O emissions quantified by both CH and EC methods in a temperate grassland under a fertilized treatment and (iii) identify the influence of fertilizer application and the environment in driving variability in N_2O emissions in space and time.

2: MATERIALS AND METHODS

2.1 Site and experimental description

The study was carried out between January and December 2019 at the Long Term Carbon Observatory experimental field site at Teagasc Environmental Research Centre, (Johnstown Castle, Co. Wexford) in the south-east of Ireland (52.30°N, 6.40°W, 67 m above sea level). This area has a temperate oceanic climate with a mean annual temperature and rainfall of 10.1°C and 1011mm respectively. The EC system was set up in the northern part of the experimental field site (Fig. 1). The field site has clay loam alfisols and consists of two paddocks (known as paddocks 10 and 11) with a collective area of 2.67 ha^{-1}. The sward composition of the grassland is dominated by perennial ryegrass (*Lolium perenne*) with white clover (*Trifolium repens*), herb-Robert (*Geranium robertianum*) and broad-leaved dock (*Rumex obtusifolius*) (Maire *et al.* 2020).

In the year prior to measurements (2018), paddock 10 was managed for silage production and paddock 11 was grazed by Holstein-Friesian dairy cows. During the measurement year (2019), there were four fertilizer applications of CAN and three silage cuts. N_2O flux measurements were performed using both CH and EC techniques and both were compared over seven comparison periods during this time (see Table 1). Six different methods were used to calculate summary N_2O flux statistics to investigate spatial (CH inside or outside the half-hourly EC footprint (FP)) and temporal differences (half-hourly EC measurements for the day or made at the same time as CH measurements) in measurements (Table 2). Mean fluxes measured from CHs were calculated using the arithmetic method and the Bayesian method (see section 2.6) to account for uncertainties in the log-normal distribution of N_2O fluxes in time.

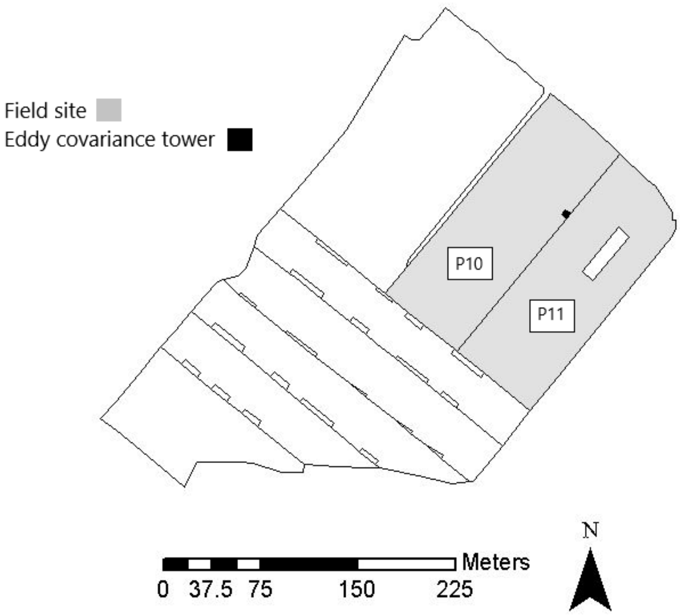

Figure 1: Map of the field site where boundaries represent paddocks (P), grey paddocks 10 and 11 represent the experimental field site (2.67 ha^{-1}) and the black square represents the eddy covariance tower.

Table 1: A summary of comparison periods where N_2O fluxes were measured by eddy covariance and static chambers. The table provides information on the length of each comparison period (*N*), management interventions including silage cuts and fertilizer application (calcium ammonium nitrate [CAN]) dates and the N loading rates in addition to key meteorological variables including cumulative rainfall (mm), average air temperature (Tair) and at 6.5cm depth soil temperature (Tsoil), water-filled pore space (WFPS), electrical conductivity (EC), and at 10 cm depth organic C, pH, ammonium (NH_4^+) and nitrate (NO_3^-).

		Management											
Comparison period	*N*	Silage cut date	Fertilizer date	Application rate	Rain	Tair	Tsoil	WFPS	EC	Organic C	pH	NH_4	NO_3
				[kg N ha^{-1}]	[mm]	[°C]	[°C]	[%]	[mS m^{-1}]	[%]		[kg ha^{-1}]	[kg ha^{-1}]
8/1/2019 - 7/2/2019	30				54.1	5.8	9	61.4	56.9			7.9	5.4
4/3/2019 - 26/3/2019	22		05/03/2019	40	67.9	7.5	10.4	70.7	60.2			8.8	4.4
1/4/2019 - 24/4/2019	23		01/04/2019	70	70.2	8.5	11.6	66	78.4	3	5.9	16.2	28.7
		14/05/2019											
4/6/2019 - 27/6/2019	23		05/06/2019	80	73.7	8.8	16.9	48.6	90	3.1	5.9	43.7	57.9
		04/07/2019											
7/8/2019 - 27/8/2019	20				100.9	15.4	20.7	44	70.3	3.2	6	2.5	19.3
2/9/2019 - 2/10/2019	30	05/09/2019	11/09/2019	40	79.3	13.7	17.8	42.9	85.1	3.2	5.9	20.4	47.5
10/10/2019 - 3/12/2019	54				247.3	8.1	12	49.7	54.1				
Total / Average	202			230	693.4	9.7	14.1	54.8	70.7	3.1	5.9	16.6	27.2

Table 2: Eddy covariance (EC) and static chamber (CH) N_2O fluxes were partitioned into six different methods to calculate summary N_2O flux statics to investigate spatial and temporal differences in measurements from both techniques.

Abbreviation	Method
EC_{All}	All EC measurements over the comparison period
EC_{CH}	EC measurements during the time of chamber measurements
CH_{All}	All CH flux measurements averaged using the arithmetic mean
CH_{Bayes}	All CH flux measurements averaged using the Bayesian mean
CH_{FP}	Daily averaged CH flux measurements within the footprint of the EC tower using the arithmetic mean
$CH_{Bayes-FP}$	Daily averaged CH flux measurements within the footprint of the EC tower using the Bayesian mean

2.2 Static chamber measurements

N_2O fluxes were measured using the closed CH method, as outlined in de Klein *et al*. Thirty square stainless-steel collars (40 cm wide, 15 cm height) were installed in September 2018 across the field site to a depth of 5-10 cm depth following a sector randomization design (Chadwick *et al.* 2014). The CH lids were 10 cm high which created a headspace of approximately 20-22 L. CHs were closed during tractor spreading of CAN fertilizer, opened immediately afterwards and subsamples of CAN fertilizer were applied at the same rate homogeneously by hand within the chamber area. N_2O fluxes were measured between 10:00h and 14:00h (GMT) to best reflect daily average N_2O emissions (de Klein *et al*. 2015). Background N_2O fluxes were measured once a week. Following CAN fertilizer applications, the measurement frequency increased to 4 measurements per week (for the first 2 weeks) and 2 times per week (for the following 2 weeks) before returning to the background (weekly) measurement frequency.

Gas samples were taken from the CH headspace over a 40-minute period at 20 minute intervals (T_0, T_{20} and T_{40}). Headspace gas measurements were extracted through a rubber septum (Becton Dickinson, Oxford, UK) using a 10ml polypropylene syringe (BD Plastiplak, Becton Dickinson) fitted with a hypodermic needle (BD, Microlance 3; Becton Dickinson). Gas samples were injected into a pre-evacuated (to -1,000 mbar) 7ml screw-cap septum glass vials (Labco, High Wycombe, UK). N_2O concentrations were analysed using gas chromatography (GC) with a detection limit of 0.05 ppm (Scion 456-GC, Kirkton Campus Livingston, UK), equipped with an electron capture detector with high purity helium as a carrier gas. Hourly fluxes in µg N_2O m^{-2} hr^{-1} were calculated by linear regression of changes in N_2O concentration within the chamber headspace between T_0 to T_{40} (Krol *et al.* 2017) Eq. (3)

$$F_{chamber} = \left(\frac{\Delta C}{\Delta T}\right) x \left(\frac{M\ x\ P}{R\ x\ T}\right) x \left(\frac{V}{A}\right)$$

Where ΔC is the change in headspace concentration of N_2O during the enclosure period in ppbv, ΔT is the enclosure period in hours, M is the molecular weight of N_2O (44.01 g mol^{-1}), P and T are the atmospheric pressure and temperature at the time of gas sampling, respectively, R is the ideal gas law constant (8.314 J K^{-1} mol^{-1}), V is the headspace volume in a closed chamber (m^3) and A is the area covered by the collar of the gas chamber (m^2). Linearity of N_2O accumulation within the chamber headspace was determined by assessing the coefficient of determination (R^2); where the R^2<0.7 flux measurements were removed from the dataset. In addition to this, CO_2 concentrations were measured adjacent to N_2O by GC, and where CO_2 concentrations showed deviations from a linear accumulation within the chamber headspace (i.e. a transition from plant respiration to photosynthesis), it was assumed there was a leak within the chamber and N_2O flux measurements were removed from the dataset.

2.3 Soil measurements

Soil temperature (^oC), electrical conductivity (mS m^{-1}) and volumetric water content (VWC %) measurements (WET sensor, Delta-T Devices Ltd, Burwell, UK) were taken at the same time as the CH flux measurements at 6.5 cm depth and 50cm from the CH location. Topsoil cores were taken a meter away from CH locations 48 hours before and 24 hours after each fertilization event, using a 10 cm depth and 1.7 cm diameter soil corer. Data derived from soil core analysis were used to characterize the key soil characteristics across the field site over the annual sampling campaign (Table 1). Soil cores were kept undisturbed and refrigerated at 4^oC until thoroughly mixed and wet sieved (4 mm). Composite subsamples were immediately taken to determine mineral N contents (NH_4^+ and NO_3^-), using 2M KCL as extractant (1:5 ratio), 1-h agitation and filtration (Whatman No. 2) following recommendations from Jones and Willet (2006). Extracts were analysed using an Aquakem 600 discrete analyser (Thermo Electron OY, Vantaa, Finland) for NH_4^+-N (Standing Committee of Analysts, 1981) and NO_3-N (Askew, 2012). The remainder of the mineral N soil subsample was oven dried at 105 ^oC over 24 hours to determine soil moisture content. The rest of the composited sample was air-dried and analysed for pH (Gilson 215 Liquid Handler, Middleton, USA) and soil organic carbon (SOC) contents (infrared CN analyser after ball-milling; LECO TruSpec, USA). Sharpened cylindrical rings (n =30; 10cm depth; 3.7 cm diameter) were used to sample the soil bulk density (BD, debris > 2mm not considered) of surface topsoil across the field site prior to commencing the experiment and subsequently, the water-filled pore space (WFPS) by dividing the VWC by the total porosity of the BD sample (Linn and Doran, 1984).

2.4 Micrometeorological measurements

An EC mast was installed with a 3-D sonic anemometer (CSAT-3, Campbell Scientific Ancillary, Logan, UT, USA) mounted at 2.2m to measure fluctuations in the 3-D wind components at a frequency of 10 Hz. A 10 m long, 10 mm inner diameter perfluoroalkoxy (PFA) tube was attached and placed 30 cm apart from the sonic anemometer in the same horizontal axis. To minimize debris and pollution obstructing the PFA tubing, a 2 mm fabric mesh was fitted approximately 2cm out from the tip of the inlet tubing. The air inlet extended to a temperature controlled trailer (161 cm x 98 cm x 127 cm) where it was connected to a quantum cascade laser (QCL) absorption spectrometer (LGR 23R N_2O/CO analyser, Los Gatos Research, California, USA) for measuring N_2O fluxes at 10 Hz with a detection limit of 0.03 ppb over a 30 minute period. The inlet tube was fitted with two in-line 2 µm filters (SS-4FW4-2, Swagelok™) and the filter threads were wrapped in polytetrafluoroethylene (PFTE) tape to minimize air leaks. Additional 2 µm and 10 µm (Los Gatos Research, California, USA) filters were fitted within the QCL at the entrance of the inlet tubing and upstream of the internal pump, respectively. A 2.4 m long and 2.5 cm wide PDTE clear suction hose with steel spiral wired rings (Tec Industry, Dublin, Ireland) connected the QCL to a dry scroll vacuum pump (XDS35i, Edwards, West Sussex, UK) which was used to draw air into the inlet and cell of the QCL with an approximate flow rate of 30 -35 standard L min^{-1}. The cell pressure was set at 85 torr and the replacement rate of air within the cell was 0.097 s^{-1}.

Ancillary sensors at the EC site included an air temperature and relative humidity probe (HMP155C, Campbell Scientific, Logan, UT, USA), two net radiation sensors (NR-Lite, Kipp and Zonen, Delft, The Netherlands), two self-calibrating soil heat flux plates installed at 5 cm soil depth (HFP01SC, Hukseflux, Delft, The Netherlands), photosynthetic active radiation (PAR) (PQS1, Kipp and Zonen, Delft, The Netherlands) and averaging soil temperature probes (TCAV-L, Campbell Scientific, Logan, UT, USA) installed at 2 cm and 6 cm depth above the soil heat flux plates. Time domain reflectometers (CS616, Campbell Scientific, Logan, UT, USA) measured soil VWC in the upper 15 cm of soil. Data from the

EC system was stored and collected from the CR3000 micrologger (Campbell Scientific, Logan, UT, USA).

2.5 Post-processing eddy covariance flux data

Ecosystem scale N_2O fluxes were continuously measured over a 365-day period in 2019 with the exception of short equipment maintenance intervals that accounted for 45 days. Raw EC data at 10 Hz was processed using the Eddypro software, version 7.0.4 (www.licor.com/eddypro). EC N_2O fluxes (µmol m^{-2} s^{-1}) were calculated as the covariance between the vertical wind speed (w) and the N_2O concentration (ρc) Eqn. (4) (Burba, 2013). To compare EC N_2O fluxes to CH N_2O fluxes, units were converted from µmol N_2O m^{-2} s^{-1} to µg N_2O-N m^{-2} hr^{-1}.

$$F_{EC} = \overline{w'\rho c'}$$

Raw data was screened and statistically evaluated according to Vickers and Mahrt (1997) for drop-outs, amplitude resolution, absolute limits, skewness and kurtosis tests for de-spiking tests. Double rotation was performed to compensate for the anemometer tilt by nullifying the average cross-stream and vertical wind components (Kaimal and Finnegan, 1994). Block averaging was used to calculate turbulent fluctuations. The time lag for N_2O was estimated using the covariance maximization procedure in two steps. First, the maximization of covariance of data over six hour chunks of sequential data was determined over a large window of 10 seconds. Second, once a steady time lag was identified throughout the measurement period, a second covariance of maximization of the same six hour data chunk was re-run over a narrower window of 0.3 seconds, using the median running timelag over a 7 day period as the mid-point. Finally, the mixing ratio data was re-paired with the wind data at a fixed timelag of 0.5 seconds based on the previous maximisation of covariance, and eddy pro was run with a fixed timelag, with fluxes calculated over a 30 minute period. Spectral attenuation effects following analytic methods described in Fratini *et al.* (2012) and Moncrieff *et al*. (2004) determined low and high-pass spectral correction factors for the data, respectively. A 5-step quality control protocol was applied for filtering bad quality N_2O fluxes. Flux data was removed from the data set if (1) less than 70% of the flux contribution came from inside of the boundaries of the field site, as determined by the analytical footprint model described by Kormann and Mexiner, (2001), (2) if flux quality control flags by Foken (2003) were category 6 or above; (3) where low turbulent conditions were present, defined as the friction velocity (u*) < 0.1 m^{-1} s^{-1} (Lognoul *et al*. 2019); (4) where the flux random uncertainty integrated over a fixed 10s correlation period was > 0.001 μmol N_2O m^{-2} s^{-1} as estimated by the method of Finkelstein and Sims (2001); and (5) where flux values were < -0.1 μmol N_2O m^{-2} s^{-1} as such values were deemed unrealistic for this field site and similarly managed grasslands (Wecking *et al*. 2020) . After filtering, 46% of measured fluxes passed the quality control procedure. N_2O flux measurements were partitioned into two dataset (1) fertilizer events, defined as the first 30 days following fertilizer application, and (2) background, defined as 30 days outside of a fertilizer event. Each dataset was gap-filled separately using a simple multivariate process based model that included: (1) rolling averages of Tair, Tsoil, WFPS and rolling sums of rainfall over 6 hr^{-1}, 12 hr^{-1}, 24 hr^{-1}, 48 hr^{-1}, 100 hr^{-1} periods (Mishurov and Kiely, 2011) where data correlated significantly with log(N_2O-N flux) as determined from a subsets regression model performed in R studio (RStudio Team, 2020); (2) days since fertilizer application; and (3) the previous and next measured flux in the dataset. The gap-filled fertilizer events and background datasets were merged, creating a gap-filled EC N_2O flux data set for the experimental year.

2.6 Data analysis

The coefficient of variation (CV) was used to describe the variability of N_2O fluxes over each comparison period for each subset of EC and CH data Eq (5):

$$CV = \left(\frac{\partial}{\mu}\right) * 100$$

where ∂ is the standard deviation and μ is the arithmetic mean, expressed in percentage. An overlay analysis was performed on ArcMap (ESRI, 2011) to identify which CH measurements were within the footprint of the EC. Using a hand-held GPS device (GPSMAP 64, Garmin, Shaffhausen, Switzerland), GPS coordinates of CH locations within the field site were measured and overlaid on images of the EC footprint (Kljun *et al.* 2015) during the time of CH measurements (Fig. 2). Comparisons between EC and CH flux measurements were made using orthogonal regression in order to avoid biases between methodologies (Jones *et al.* 2011). CH hourly fluxes were assumed to be representative of daily emissions and were used to calculate the daily mean N_2O flux. In order to approximate the total N_2O produced from CAN, cumulative fluxes by CH and EC were calculated by linear interpolation between daily mean fluxes. Cumulative fluxes were used to derive emission factors (EFs) from CAN Eq. (6). EFs represent the % of N_2O-N emitted from CAN applied.

$$\mathrm{EF} = \left(\frac{[\mathrm{N_2O}_{\ \mathrm{CAN}} - \mathrm{N_2O}_{\ \mathrm{Control}}]}{\mathrm{N\ applied}}\right) * 100$$

Where N_2O_{CAN} is the cumulative N_2O emissions (kg N_2O-N ha^{-1} yr^{-1}) from CAN, $N_2O_{Control}$ is the cumulative N_2O emission (kg N_2O-N ha^{-1} yr^{-1})from a control (in this study, defined as 0), N applied is the rate of CAN applied (kg N ha^{-1} yr^{-1}). In order to compare field scale CH flux measurements with ecosystem scale EC flux measurements, daily mean CH measurements were upscaled using a Bayesian approach (Wild *et al.* 1996). Markov Chain Monte-Carlo (MCMC) simulations were performed using Gibbs sampling to estimate the posterior distribution of μ by combining the prior data with this study's data. MCMC simulations were run on the freely-available JAGS software (Plummer, 2015). The prior dataset selected for this study was from Cowan *et al.* (2017) as log-normal distributions from both datasets overlapped well. The posterior distribution is primarily influenced by the data, except where the data does not possess a log-normal distribution and therefore cannot constrict the fit of μ_{log} and σ_{log} variables. The prior prevents the range of μ from expanding into unrealistic ranges by reducing the influence high, outlier values have on μ. The Bayesian method was used to estimate μ and the 95% confidence intervals of the posterior distribution from CH measurements (see Table.3).

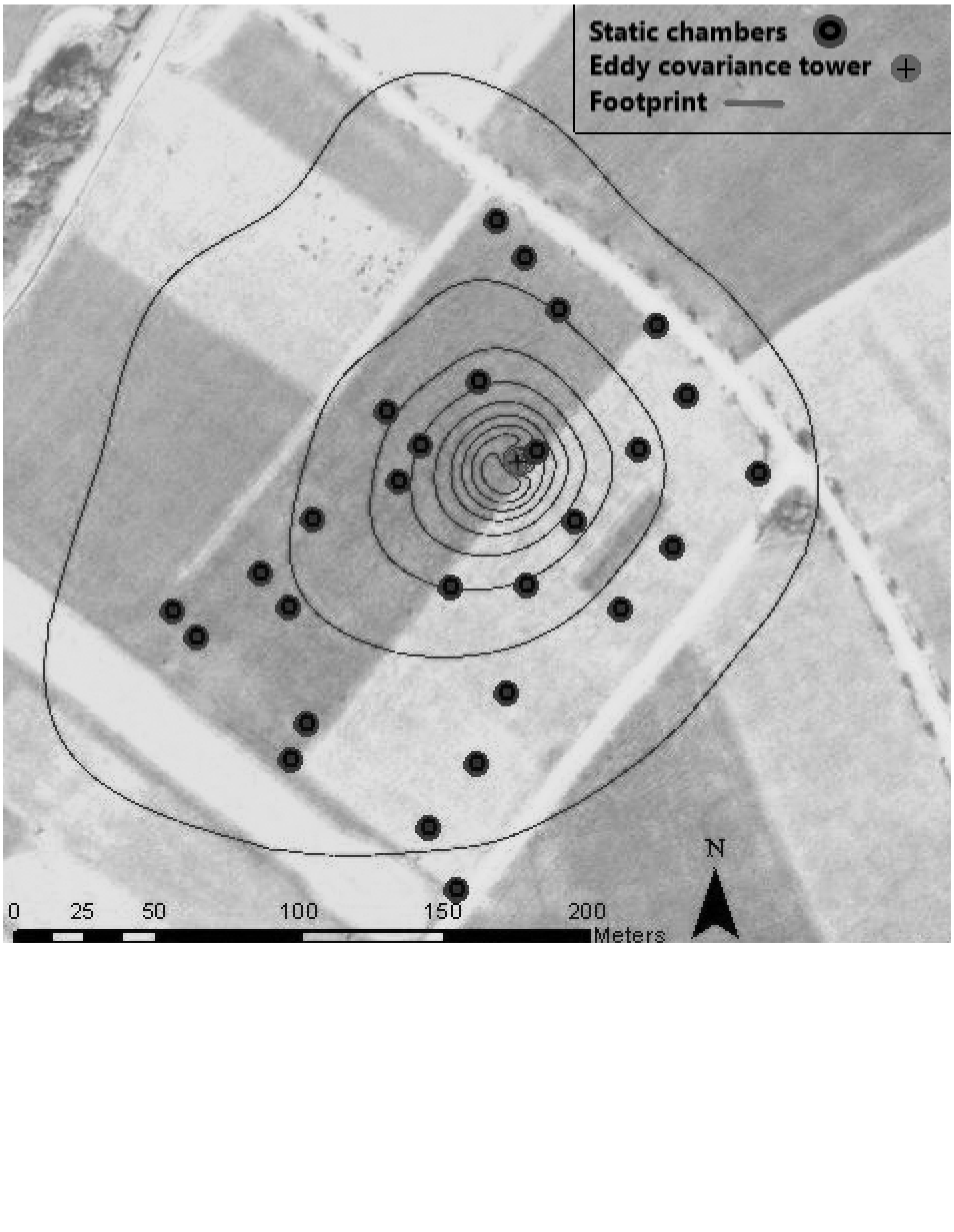

Figure 2: Static chamber (CH) locations within the eddy covariance (EC) footprint for 2019 (Kljun *et al.* 2015) where black circles with rings represent CH, the grey circle with a cross is the EC tower and grey contour lines represent the footprint of the EC where the outer to inner contour line represents 90 % – 10 % of the footprint, respectively

3: RESULTS

3.1 Meteorological data

Meteorological data measured at the EC station can be seen in Fig. 3. Mean daily air temperature ranged from 0.9°C in January to 18.2°C in July, with an annual mean temperature of 10.3°C (Fig. 3a). Soil temperature at 6cm depth was greatest in July and lowest in December with values of 20.0°C and 1.7°C, respectively. WFPS measured in the upper 15 cm of the soil, peaked in November at 74.9% and was lowest in September at 39.6% (Fig. 3b). Prolonged dry periods (greater than 14 consecutive days at <50% WFPS) were observed in July and September. The total annual rainfall for the experimental period was 958.4 mm (Fig. 3c), with heavy rainfall events of 40.1 mm and 30.7 mm occurring in August and April, respectively.

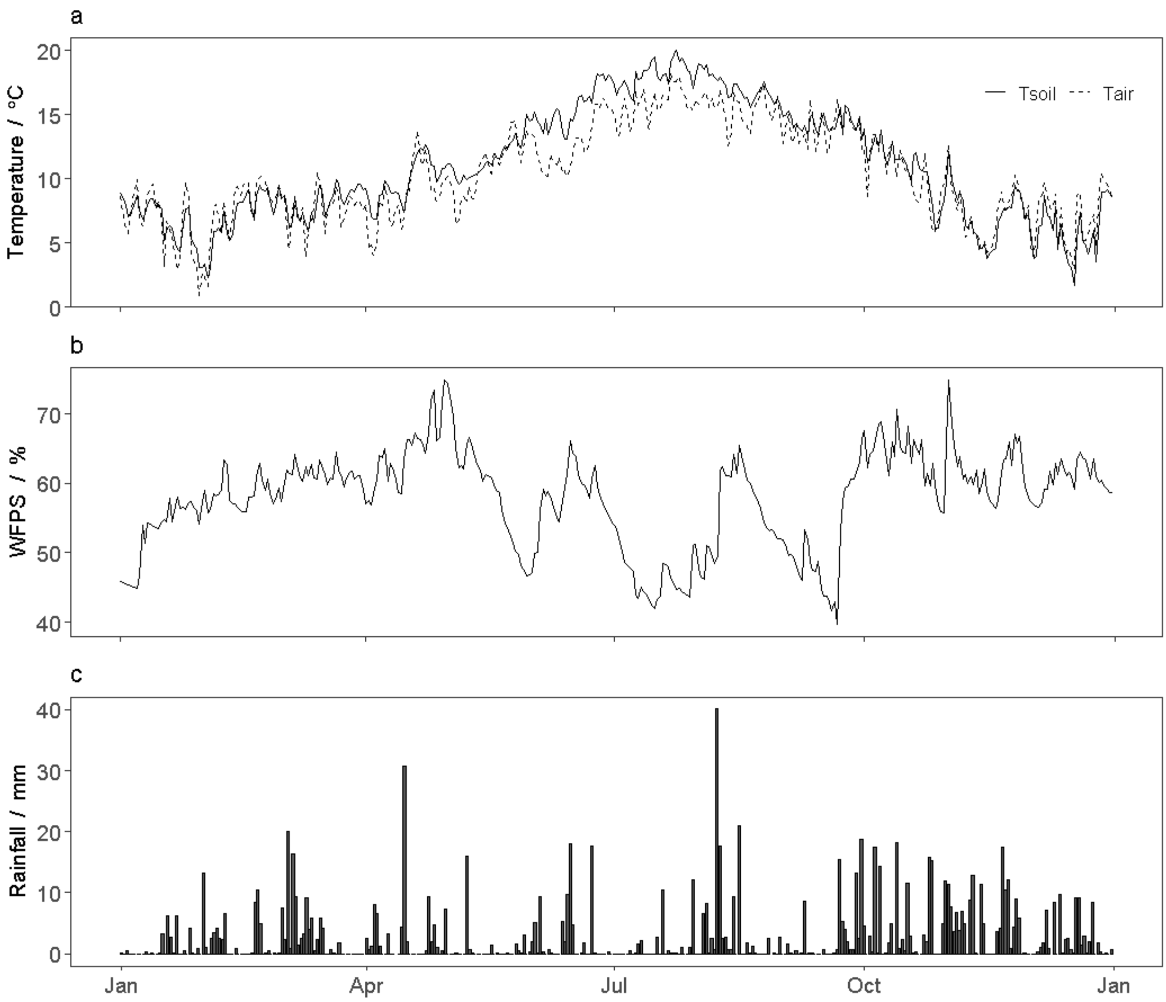

Figure 3: Meteorological data measured at the field site from January 2019 to December 2019 where panels (a), (b) and (c) show mean daily, soil temperature (°C) (Tsoil) (solid line) , and air temperature (°C) (Tair) (dashed line), water-filled pore space (WFPS %), and rainfall (mm) respectively.

3.2 Observed fluxes of N_2O using chamber and eddy covariance methods

All N_2O-N fluxes measured by both CH and EC exhibited a log-normal distribution throughout the year (Fig. 4). Measured N_2O-N emissions from both techniques increased exponentially in the days immediately following fertilizer application (Fig. 5). Fluxes returned to background magnitude (defined as 48 N_2O-N μg m^{-2} hr^{-1} which represents the 85% quantile for flux measurements made 30 days post fertilizer application) between 4 and 29 days. The maximum mean daily N_2O-N fluxes observed were 814.76 μg N_2O-N m^{-2} hr^{-1} using EC technique and occurred 18 days post- summer fertilizer application and was preceded by a heavy rainfall event (17.6 mm). Maximum mean daily N_2O-N fluxes measured by CH were observed in spring at 538.89 μg N_2O-N m^{-2} hr^{-1}, also coinciding with a heavy rainfall event (20.9 mm). Delayed peaks in N_2O-N emissions were also measured during autumn, with peak emissions of 417.14 μg N_2O-N m^{-2} hr^{-1} (CH) and 313.22 μg N_2O-N m^{-2} hr^{-1} (EC) occurring 31 days post application, during which the WFPS increased from 48.77% to 63.85% (Fig. 3b). Minimum daily averaged N_2O flux measurements represented a zero flux from the system and were observed in winter at -0.14 μg N_2O-N m^{-2} hr^{-1} and -0.40 μg N_2O-N m^{-2} hr^{-1} for EC and CH techniques, respectively.

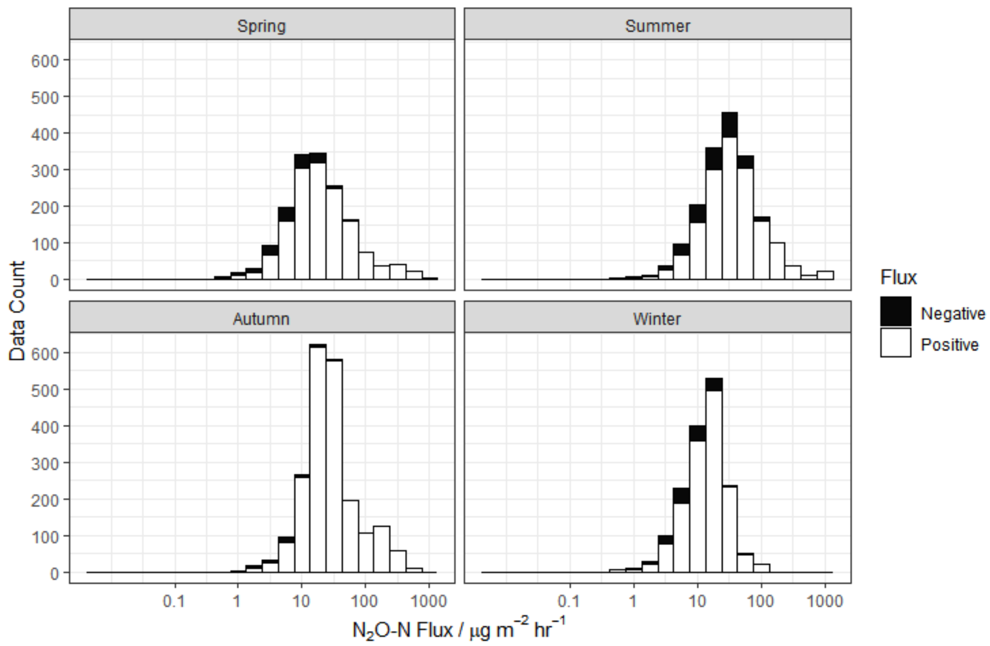

Figure 4: Frequency distribution of collective N_2O fluxes measured from both chambers and eddy covariance in 2019 for each season where spring fluxes were measured in February, March and April, summer fluxes were measured in May, June and July, autumn fluxes were measured in August, September and October and winter fluxes were measured in November, December and January. N_2O fluxes are shown on a log-transformed axis but real values on the axis. Negative fluxes are shown on a positive scale but coloured black.

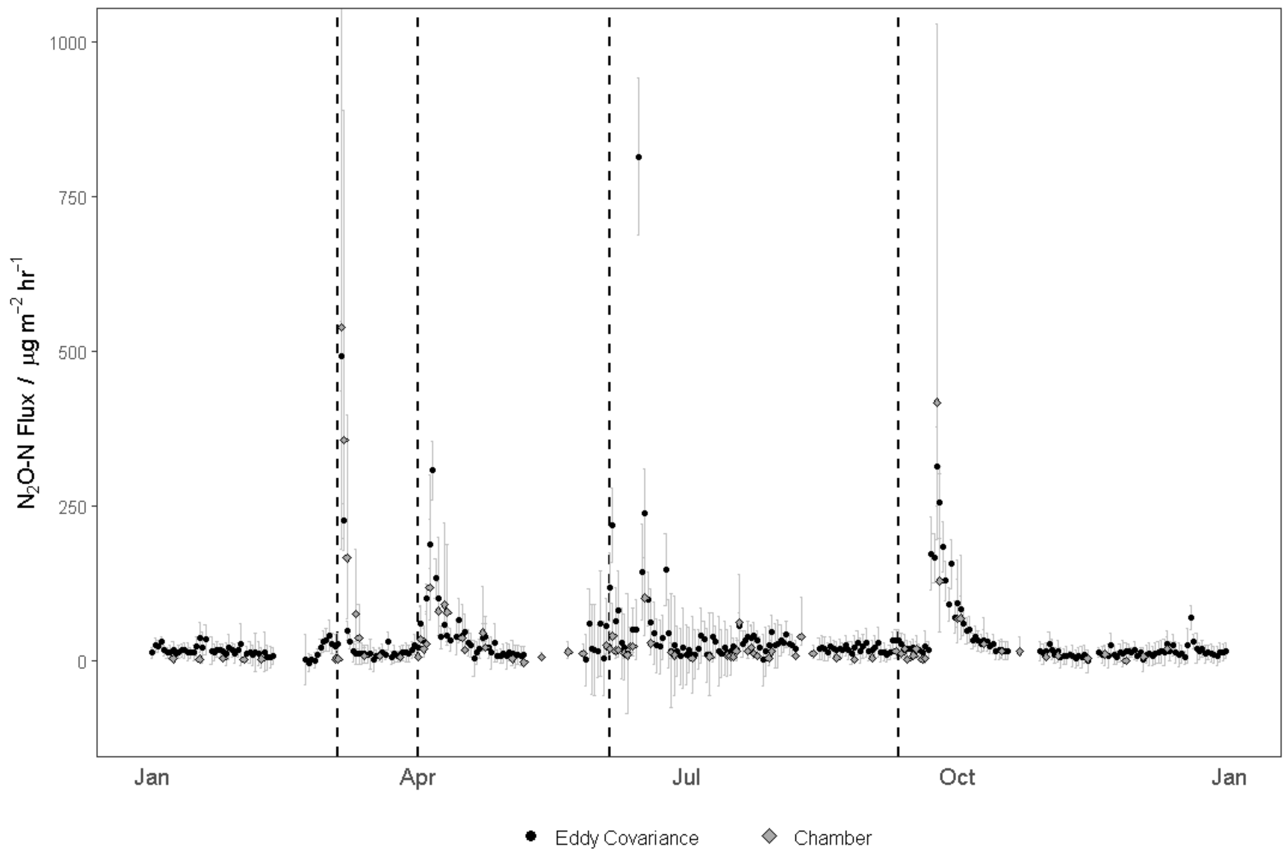

Figure 5: 2019 N_2O-N fluxes where black circles represent mean daily eddy covariance flux measurements, grey diamonds represent mean daily chamber flux measurements, grey lines represent the 95% confidence interval of flux measurements, and broken lines mark the date of fertilizer application.

3.3 Comparison of chamber and eddy covariance fluxes

Linear comparisons between subsets of daily averaged EC and CH (see Table 1) N_2O flux measurements from the comparison periods (see Table 2 for dates) are shown in Fig. 6. Summary statistics on flux measurements for each subset for each comparison period are shown in Table 3. Over the individual comparison periods, CH measurements were within the range of EC measurements. The most robust relationship between CH and EC measurements was for EC_{CH} and CH_{FP} (R^2 = 0.81) (Fig. 6d), where both methods were measuring N_2O fluxes over the same space and time, EC_{CH} and CH_{All} (R^2 = 0.79) (Fig. 6b) and EC_{CH} and CH_{Bayes} (R^2 = 0.80) (Fig. 6f) where EC measurements made during the time of CH measurements are in close agreement with CH measurements where the sample size was large (n ≈ 30) and the log-normal distribution of the sample size was accounted for. This suggests that temporal alignment between techniques was more import than spatial alignment for comparable flux measurements. The weakest relationships involved smaller subsets of CH data calculated by the Bayesian method (EC_{All} vs $CH_{Bayes\text{-}FP}$ R^2= 0.45 [Fig. 6g]; EC_{CH} vs $CH_{Bayes\text{-}FP}$ R^2 = 0.36 [Fig. 6h]). Agreement between subsets of CH and EC fluxes, was primarily driven by a few high flux measurements following fertilizer applications, which made up only a small portion of the dataset (15%). For smaller subsets for daily averaged CH measurements inside the footprint of the EC tower, the Bayesian method produced asymmetrical error bars. Where flux values were greater than 115 µg N_2O-N m^{-2} hr^{-1}, error bars were often several orders of magnitude larger than the estimated flux, due to the inability to constrain an arithmetic mean from a log-normally distributed data set with a low number of measurement points. In general, variability in N_2O-N flux measurements (CV %) was greater for N_2O-N fluxes measured by CH compared to EC over the comparison periods (Table 3).

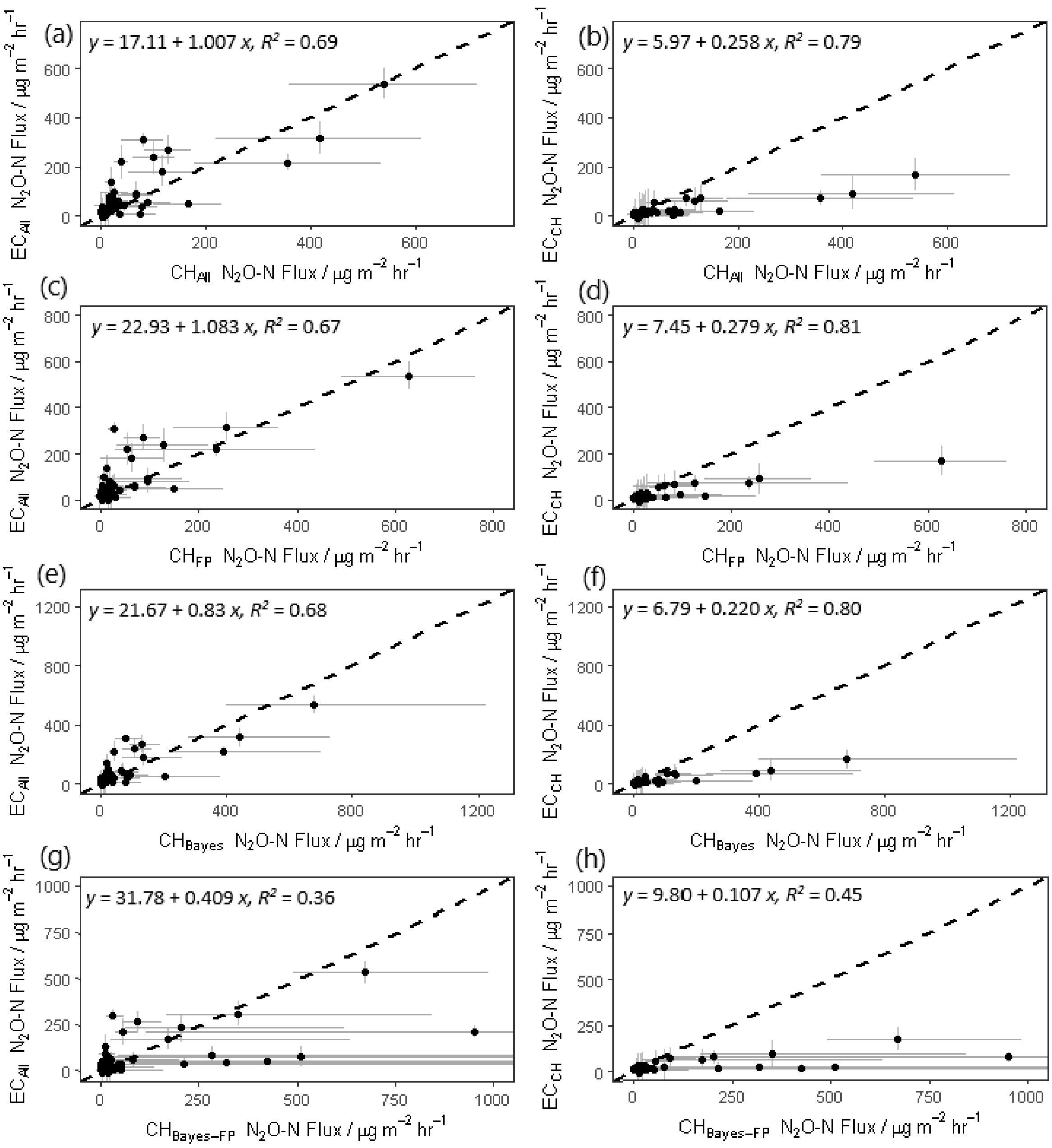

Figure 6: Comparison plots for (a) all half-hourly eddy covariance (EC) N_2O-N fluxes (EC_{All}) and all daily averaged chamber (CH_{All}) N_2O-N fluxes and (b) EC measurements during the time of chamber measurements (EC_{CH}) and CH_{All}, (c) EC_{All} and daily averaged chamber flux measurements within the footprint of the EC tower (CH_{FP}), (d) EC_{CH} and CH_{FP}, (e) EC_{All} and all chamber flux measurements daily averaged using the Bayesian mean (CH_{Bayes}), (f) EC_{CH} and CH_{Bayes}, (g) EC_{All} and daily averaged chamber flux measurements within the footprint of the EC tower using the Bayesian mean ($CH_{Bayes\text{-}FP}$) and (h) $EC_{T.ch}$ and $CH_{Bayes\text{-}FP}$. Black bars represent the 95% confidence

interval error of half-hourly EC N_2O-N flux measurements, grey bars represent the 95% confidence interval error of daily averaged chamber N_2O-N flux, and the broken grey line represents the 1:1 ratio. Ranges on the error bars have been curtailed for showing clearer comparisons between both techniques. See Table A.1 and Table A.2 in the Appendix for full values.

Table 3: Summary statistics of N_2O flux measurements from chambers (CH) and eddy covariance (EC) for seven comparison periods. No. of samples represents the number flux measurements made during the measurement period. Methods used for calculating N_2O fluxes for each comparison period included all daily averaged chambers flux measurement (CH_{All}) and daily averaged chamber flux measurements from chambers that were located within the EC footprint (CH_{FP}), calculated using both arithmetic and Bayesian methods, all half-hourly EC flux measurements (EC_{All}) and half-hourly EC flux measurements that were made during the time of chamber measurements (EC_{CH}). The Coefficient of Variation (CV%) is averaged over all flux measurements (either daily arithmetic averages or half-hourly flux measurements).

				N_2O-N flux µg m^{-2} hr^{-1}						
Comparison period	#	Method	N	Arithmetic			Bayesian			
				95% C.I.			95% C.I.			
			no. of samples	min	max	mean	min	max	mean	CV%
8/1/2019-7/2/2019	1	CH_{All}	105	1.77	2.58	2.18	1.77	2.60	2.18	97.57
		CH_{FP}	43	1.62	2.69	2.15	1.61	2.72	2.16	82.54
		EC_{All}	94	59.89	62.01	13.89				118.25
		EC_{CH}	12	1.72	46.48	15.74				74.29
4/3/2019-26/3/2019	2	CH_{All}	295	79.04	139.71	109.38	67.67	100.60	82.77	243.02
		CH_{FP}	87	56.94	147.98	102.46	54.82	120.56	82.03	211.41
		EC_{All}	367	20.07	1088.96	96.29				202.40
		EC_{CH}	31	1.08	640.27	97.25				191.77
1/4/2019-24/4/2019	3	CH_{All}	353	35.05	43.91	52.77	33.19	44.32	38.46	160.96
		CH_{FP}	59	12.49	23.37	34.24	15.21	30.14	22.04	125.63
		EC_{All}	341	34.48	345.85	86.17				99.25
		EC_{CH}	39	15.53	304.51	70.82				76.86
4/6/2019-27/6/2019	4	CH_{All}	390	20.83	29.39	25.11	21.03	25.81	23.34	171.60
		CH_{FP}	94	22.56	48.47	35.51	26.30	39.49	32.36	180.28
		EC_{All}	321	81.07	418.44	104.15				92.43
		EC_{CH}	43	58.38	329.71	80.72				109.07
7/8/2019-27/8/2019	5	CH_{All}	150	6.71	11.56	16.41	8.14	13.04	10.50	184.70
		CH_{FP}	39	6.12	9.63	13.14	6.43	13.48	9.73	90.06
		EC_{All}	99	12.10	51.02	18.11				53.36
		EC_{CH}	14	12.10	35.69	18.09				79.29
2/9/2019-2/10/2019	6	CH_{All}	388	38.24	55.89	73.54	35.65	48.07	41.48	241.23
		CH_{FP}	123	29.90	46.13	62.35	31.18	51.53	40.46	147.25
		EC_{All}	339	29.85	539.44	102.59				126.31
		EC_{CH}	58	2.68	403.32	79.56				139.07
10/10/2019-3/12/2019	7	CH_{All}	299	8.36	10.79	13.22	8.63	12.02	10.29	162.31
		CH_{FP}	69	9.42	14.57	19.72	10.25	19.46	14.53	110.61
		EC_{All}	283	46.48	61.30	17.17				90.33
		EC_{CH}	34	46.48	41.44	15.29				129.07

3.4 N_2O fluxes and environmental variables

Diurnal patterns in N_2O emissions were not observed suggesting that changes in temperature between day and night and potential root exudation of carbon during photosynthesis (and therefore changes in soil carbon availability), did not have a significant control on N_2O production. Mean daily log(N_2O-N) emissions showed the greatest variability within a temperature range of 7°C and 15°C, across WFPS values of 55% to 65% and with increasing cumulative rainfall. Rolling averaged data presented in Table 5 best explained the variability in log(N_2O-N) fluxes from the respective environmental factor, as determined by a subset regression model. The full output of this model can be seen in Table A.3. Correlations with background log(N_2O-N) fluxes (30 days outside of fertilizer events) and WFPS, rainfall, air and soil temperature were weak but improved in the 30 days following fertilizer application. Environmental variables in Table 5 were significantly correlated ($p < 0.05$) with log(N_2O-N) flux measurements.

Table 5: Variance in log(N_2O-N) fluxes explained by a subset regression model on water-filled pore space (WFPS%), rainfall (mm) air temperature (T_{air} °C) and soil temperature (T_{soil} °C) over rolling averages of 48hrs^{-1} and 100 hrs^{-1} periods in the 30 days following fertilizer application (Fertilizer) and in the 30 days outside of fertilizer applications (Background).

Variable	Treatment	R^2
WFPS 48 hr^{-1}	Fertilizer	0.50
Rainfall 100 hr^{-1}	Fertilizer	0.50
T_{soil} 100 hr^{-1}	Fertilizer	0.48
T_{air} 100 hr^{-1}	Fertilizer	0.43
WFPS 100 hr^{-1}	Background	0.31
Rainfall 48 hr^{-1}	Background	0.31
T_{soil} 48 hr^{-1}	Background	0.31
T_{air} 100 hr^{-1}	Background	0.27

3.5 Modelled eddy covariance N_2O emissions

A linear multivariate regression model consisting of (1) WFPS, rainfall, air and soil temperature over 6 hr^{-1}, 12 hr^{-1}, 24 hr^{-1}, 48 hr^{-1} and 100 hr^{-1} periods (Table. A.3); (2) time since fertilizer application; and (3) the previous and next available measured flux value between the gap in the dataset, was used to gap-fill EC flux measurements, and calculate the associated uncertainty. Where correlation between environmental variables and fluxes were found to be significant ($p<0.05$), these were included in the gap-filling model (see Table A.4 for a summary of the model output). Modelled and measured flux values showed a strong correlation ($R^2 = 0.92$) (Fig. A.1). The upper and lower uncertainty surrounding modelled N_2O-N flux values was expressed as the 2.5% and 97.5% confidence intervals (Fig. 7). Uncertainty was greatest for high N_2O flux values (particularly around fertilizer events) compared to flux measurements outside of fertilizer events.

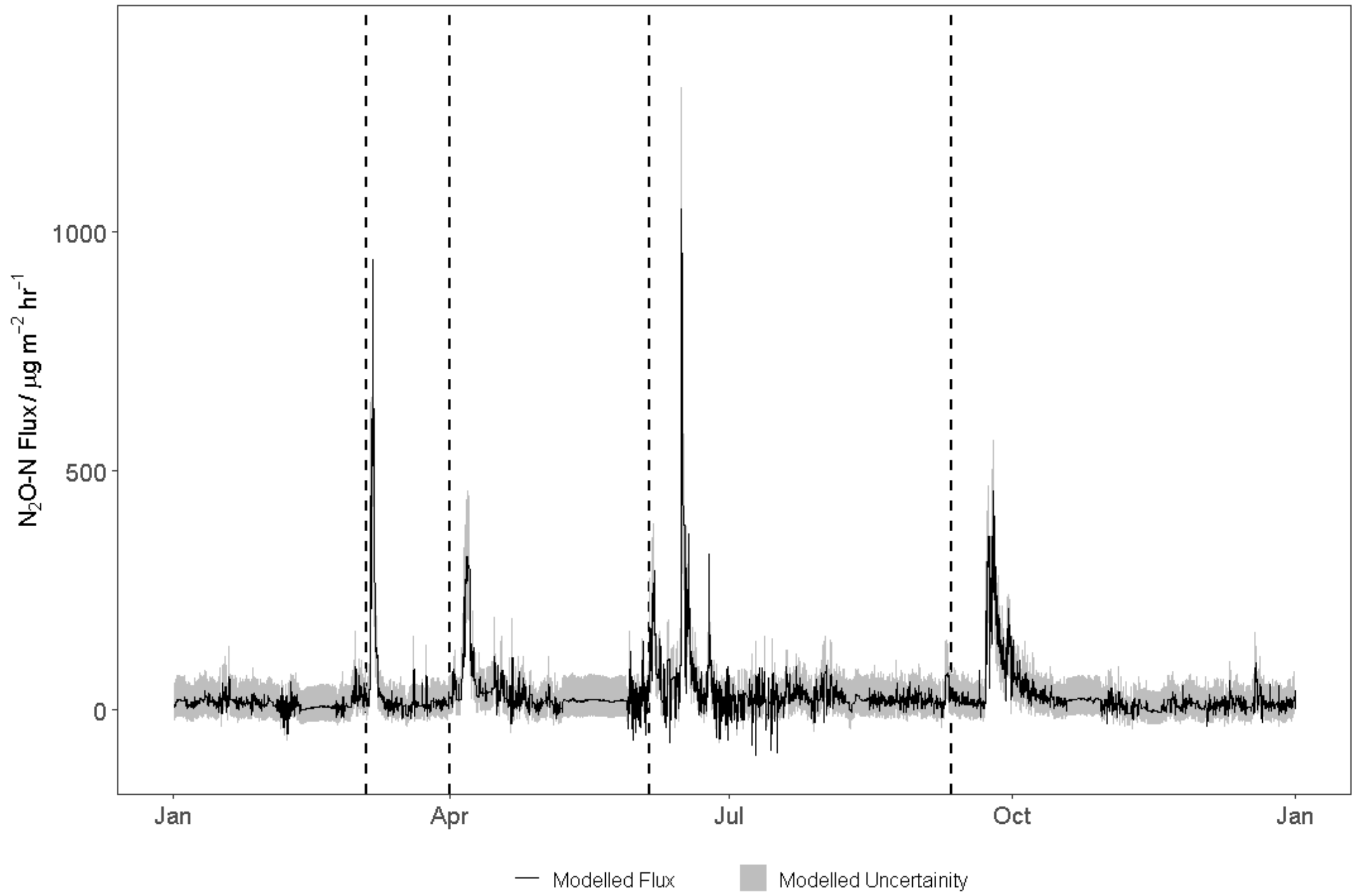

Figure 7: Linearly modelled half-hourly N_2O-N flux values (black line) and uncertainty (shaded areas), which represents the upper (97.5%) and lower (2.5%) limits of the modelled flux value. The dashed lines represent fertilizer applications (see Table 2 for dates).

3.6 Measured Cumulative fluxes

Cumulative N_2O fluxes were calculated for each subset of EC and CH data over each comparison period (see Table A.5 for a summary). Cumulative N_2O emissions measured by EC were greater than cumulative emissions measured by CH. Cumulative N_2O emissions for EC_{All}, CH_{All} and CH_{Bayes} were lowest in the winter (comparison #1) and greatest in the autumn (comparison #6). Cumulative emissions from $CH_{Bayes\text{-}FP}$ were consistently higher than other CH methods due to the small sample size and high variance in the data. Modelled flux values were used to gap-fill measured EC flux values in order to calculate cumulative emissions for the field site for 2019. Cumulative annual N_2O-N fluxes from January to December were 3.35(± 0.5) kg N ha^{-1}, 2.98 (± 0.17) kg N ha^{-1}and 3.13 (± 0.24) kg N ha^{-1}, which translated to EFs of 1.46%, 1.30% and 1.36% for EC, and CH fluxes by the arithmetic and Bayesian method, respectively (Fig. 8). Cumulative fluxes between CH (both arithmetic and Bayesian) and EC were quite similar overall, with both methods showing four distinct emission events following fertilizer applications. EC cumulative emissions were consistently lower than CH emissions from March to mid-June but following the June fertilizer application, higher cumulative flux values were observed by EC compared to CH for the duration of the year.

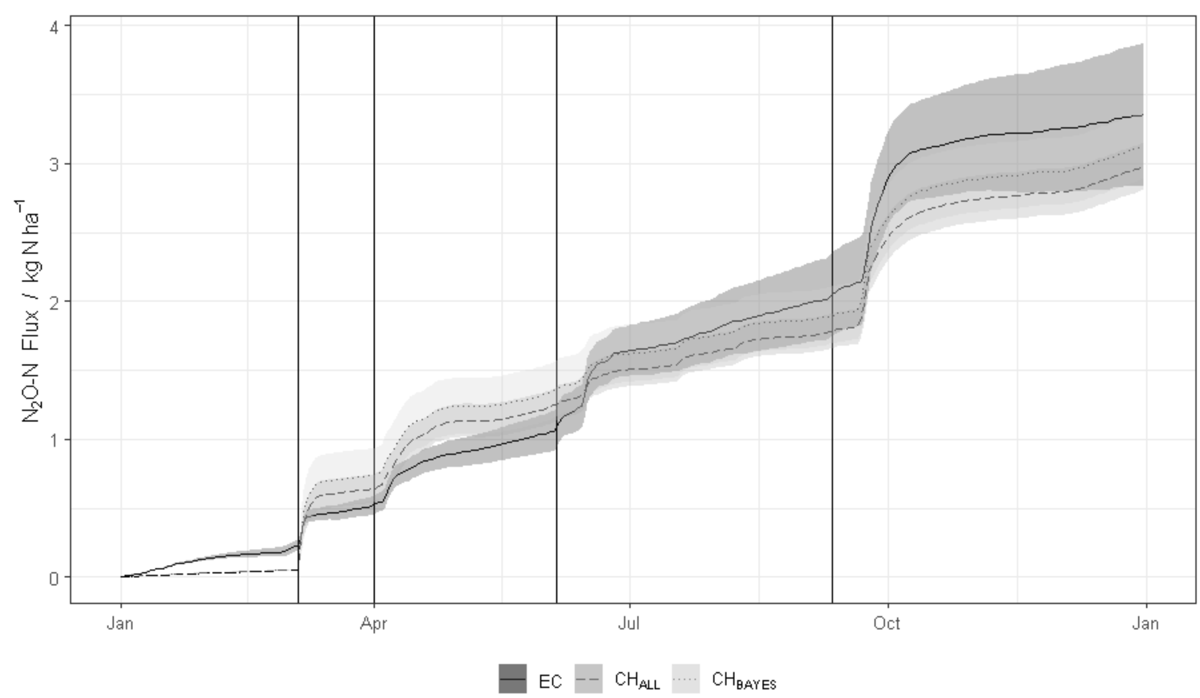

Figure 8: Cumulative daily averaged N_2O-N fluxes (black line) and uncertainty (shade) (expressed as the least squares) from January to December 2019 by eddy covariance (solid line) and chambers by the arithmetic (dashed line) and Bayesian method (dot-dashed line) and the solid vertical lines represent fertilizer applications.

4. DISCUSSION

4.1 Drivers of N_2O fluxes observed

The range of N_2O fluxes observed in this study from CH and EC methods are comparable with those at other fertilized temperate grassland sites (e.g., Cowan *et al*. 2020 for EC, Rafique *et al*. 2011 for CH). N_2O emissions were greatest in the summer and autumn following fertilizer application where extended dry periods (< 50% WFPS) were followed by heavy rainfall events (≥ 17 mm) and which led to higher WFPS values (> 60%). Similar temporal trends in N_2O emissions following fertilizer application have been documented in cropland sites (Waldo *et al.* 2019), restored grasslands (Merbold *et al.* 2020) and at various soil systems (Scherbak and Robertson, 2019). While N_2O emission events often coincided with the climatic conditions described above, peak emission events were driven by management. The variability in N_2O emissions was better explained by WFPS, air and soil temperature and rainfall following fertilizer application ($R^2 \leq 0.50$) compared to outside of management ($R^2 \leq 0.31$). Similar drivers of variability in N_2O emissions were identified in Krol *et al.* (2016) and Maire *et al.* (2020). N inputs from fertilizer in excess of plant demands can result in N losses of up to 50% (Fageria and Balingar, 2005), where residual N accumulates in soils. N-fertilizers create peak N_2O emission events by creating hotspots of N_2O through the introduction of substrates for denitrification (NH_4^+ and NO_3^-) into the soil, where by emissions of N_2O increase with greater soil NO_3^- (Zanatta et al. 2010). Increases in soil NH_4^+ and NO_3^- were observed following fertilizer application (Table 1), with the highest mineral N content following the June fertilizer application (43.7 kg ha^{-1} NH_4^+ and 57.9 kg ha^{-1} NO_3^-), which coincided with the greatest emission event of the entire experimental period at 814.76 μg N_2O-N m^{-2} hr^{-1} .

4.2 Comparison of chamber and eddy covariance flux measurements

CH and EC flux measurements were most comparable when flux measurements were high (>115 μg m^{-2} hr^{-1}), the CH sample size was large for a given day (n ≥ 15) (for both the arithmetic and Bayesian approach) and when EC and CH measurements were taken over the same area and time (i.e CH flux measurements made in the EC footprint and EC flux measurements made during the time of CH measurements). This agreement between EC and CH fluxes has been observed in previous studies (Christensen *et al.* 1996; Jones *et al.* 2011; Laville *et al*. 1997). Using the arithmetic mean when all CH measurements were considered (n ≈ 30) was sufficient in estimating the sample mean and comparable with daily mean EC flux values (EC_{CH} and CH_{All} (R^2 = 0.79) (Fig. 6b)). This is because the arithmetic sample mean will not deviate systemically from the population mean where the sample size is large and variance is low. However, as a large sample size is required (which is not always the case in CH flux studies - Hyde *et al.* 2016; Krol *et al.* 2017; Maire *et al.* 2020; Wecking *et al.* 2020), the arithmetic mean is considered an unreliable estimator of the true flux mean within a sample (Levy *et al.* 2017). Where the sample size is small and the variance is large (as is typical of N_2O flux data), the arithmetic method will typically underestimate the sample mean as infrequent, high flux values will often be absent from the sample. Where high flux values are included in the sample, the arithmetic mean will typically overestimate the sample mean. The Bayesian approach on the other hand, reduces some of the bias in N_2O flux measurements by accounting explicitly for the log-normal distribution and as a result providing realistic ranges of uncertainty within flux measurements. Where the CH sample size was small on a given day ($n \leq 5$) (i.e. when selecting CH flux measurements that are only in the EC footprint), the Bayesian approach produced larger, more asymmetrical uncertainties compared to the arithmetic method. In this instance, N_2O flux measurements did not meet the expectations based on the Bayesian model (i.e flux measurements showing a peak and decay pattern or multiple peaks or a large sample size with low variance) (Levy *et al.* 2017) and therefore, the N_2O flux data collected was not sufficient for accurately capturing the existing variability of N_2O fluxes.

Over the 86 days where both EC and CH measurements were compared, mean daily EC flux measurements were greater than CH flux measurements for a total of 63 days. Similar to the findings in this study, Wang *et al.* (2013) showed that CH N_2O flux measurements were lower than EC flux measurements by 17-20% from a cotton field. However, numerous studies have reported contrasting results. For example, Philate *et al.* (2005) found CH N_2O flux measurements were consistently greater than EC measurements and Jones *et al.* (2011) found that 70% of N_2O fluxes measured by EC were within the range of CH N_2O measurements in a grassland system, although this varied seasonally. Likewise, disagreement between EC and CH flux measurements have also been observed for CO_2 respiration rates, both in agri-ecosystems (Schrier-Uikl *et al.* 2010) and peatland sites (Cai *et al.* 2010). Disparities in flux measurements from both CH and EC can be the product of the limitations of the methods themselves. The CV was frequently greater in CH measurements compared to EC measurements due to the small scale variability detected in CH measurements. CH flux measurements represent single point measurements in space and time and, as a result, sudden dynamic variations in emissions due to either management or weather events for example, are not always quantified (Kroon *et al.* 2008). However, EC provides continuous, high frequency measurements and is therefore capable of capturing high emission events derived from hotspots and hot moments of N_2O. For example, two days post fertilizer application in March and in conjunction with a cumulative rainfall event of 27.3 mm over this period, daily average EC emissions were 219.02 µg N_2O-N m^{-2} hr^{-1}, while CH fluxes measured at midday and integrated as a daily average were 36.63 µg N_2O-N m^{-2} hr^{-1}. Moreover, the footprint of the EC tower may not always overlap with the location of where CH measurements are made and therefore take measurements over different sources of N_2O emissions, for example, in Fig. 2 70% of the EC flux footprint contribution does not encompass CH locations in the far South-West region of the field site.

In addition, EC measurements are completely *in situ* and thus, avoid artefacts caused by enclosure within a CH which are prone to under or over estimating the soil derived flux (Davidson *et al.* 2002). Such artefacts are caused by a) pressure differentials (Venturi effect) when lids are closed or in windy conditions, b) alterations in the boundary layer conditions and disturbance of diffusion gradients which can affect canopy coupling to the atmosphere within the CH, c) increases in temperature which can impact on both microbial processes and increase N_2O dilution via increased humidity (Davidson *et al.* 2002, Rochette & Hutchinson 2005, Bain *et al.* 2005, Bertora *et al.* 2018, Clough *et al.* 2020).

4.3 Gap-filling N_2O flux data

Unlike CO_2 fluxes, there are no robust, validated process-based models available for gap-filling N_2O fluxes (Moffat *et al.* 2007). Emissions of N_2O are primarily controlled by N inputs (in the form of NH_4^+ and NO_3^-) into the system (Harty *et al.* 2016), as well as soil physical and microclimatic properties such as WFPS (Davidson *et al*. 2000), temperature (Butterbach-Bahl and Dannenmann, 2011), texture (Tan *et al*. 2009) and porosity (Choudhary *et al*. 2002). While repeated measurements of these variables are feasible, in many cases continuous high frequency measurements (both spatially and temporally) are too costly or logistically not viable. Commonly used methods for gap-filling N_2O fluxes include linear interpolation (Mishurov and Kiely, 2011), 30-day running medians (Merbold *et al*. 2020) and general additive models (Cowan *et al.* 2020). While these methods have been accepted within the flux community, they should be used with due consideration for any potential limitations. Such gap-filling approaches for N_2O measurements are either too simplistic in approach, prone to large uncertainties or where a model is applied, are subject to overfitting and multicollinearity, which can reduce the sensitivity of model predictions by underestimating the variance of the fitted modelled parameters (Dorich *et al.* 2020). Here we proposed a multi-variate linear model that incorporates environmental data where the temporal pattern in the data is retained in order to account for 'emission events' over time and in doing so, provides an empirical method for interpolating between data points. The relatively high data coverage, with limited gaps exceeding a few hours and not during fertilization events (or the 30 days after), helped to reduce the uncertainties in this study. Though it is important to note that while this model was successful in gap-filling N_2O flux measurements in this study, it incorporates environmental and management data which are site-specific, and therefore may not be as successful where the experimental site is under a different management, climate and where the gaps in the data are more common. In order to further reduce uncertainties in gap-filling N_2O fluxes, we need to enhance our understanding of microbial communities and their role in N_2O production (Thompson *et al.* 2016) and implement methods that can facilitate this at high resolutions, both spatially and temporally. As flux datasets become larger, the use of neural networks (NN) for data-driven predictive modelling of N_2O will become more viable (Dorich *et al.* 2020).

4.4 Cumulative N_2O fluxes and emission factors

Cumulative CH N_2O fluxes are derived from non-continuous measurements commonly made during the daytime, expressed as a daily average and linearly interpolated between days (Dorich *et al.* 2020). Where the frequency of measurements are low, the uncertainty in the integration of measurements for cumulative flux estimates increases. As N_2O is highly variable in space and time, reducing the uncertainty in interpolating between measurement points requires many and frequent flux measurements (Lammirato *et al.* 2018).

In this study, cumulative N_2O emissions by CH were greater than EC cumulative fluxes prior to the June fertilization event, but following this event, cumulative emissions measured by EC were consistently greater than CH. Daily emissions of N_2O measured by EC peak following the June fertilizer event at 814.76 μg N_2O-N m^{-2} hr^{-1} following a rainfall event of 17.6 mm. Daily emissions captured by CH during this period were considerably lower at 7.74 μg N_2O-N m^{-2} hr^{-1}, suggesting that both frequency and the time of CH measurements (midday) were not sufficient to capture the N_2O emission event observed in the EC measurements. Similarly, cumulative EC emissions from the time of CH emissions (EC_{CH}) (typically between 10:00am and 2:00pm) were 19% - 38% (depending on the comparison period [Table 6]) lower than cumulative EC emissions from the entire day (EC_{All}). While studies have shown higher N_2O emissions in the midday (Liáng *et al.* 2018; Shurpali *et al.* 2016), our results suggest that only considering midday flux measurements could under-estimate the cumulative flux, and the magnitude of this under-estimation could be greater following fertilizer application. We recommend that daily CH flux measurements should be made at least twice a day (mid-day and night), with increasing frequency following N-inputs into the system and rainfall events. Ideally, an automated chamber system should be used for comparison with EC flux measurements, where continuous flux measurements are available over high temporal resolutions. Annual cumulative N_2O fluxes measured by EC (3.35kg N ha^{-1}) were more similar to CH cumulative fluxes determined using the Bayesian method (3.13 kg N ha^{-1}) compared to the arithmetic method (2.98 kg N ha^{-1}). The Bayesian method captures the post-fertilization temporal pattern of peak and decay that is commonly observed in N_2O flux measurements (Cowan *et al.* 2019; Levy *et al*. 2017) by accounting for the log-normal distribution of the data. In doing so, the Bayesian mean will not attribute equal weight to all data points, as the arithmetic method does, and is therefore less likely to over or under-estimate the sample mean and will provide a more robust mean for a log-normally distributed dataset. EFs from this study for EC and CH derived using arithmetic and Bayesian methods were 1.46%, 1.30% and 1.36%, respectively which is higher than the Intergovernmental Panel on Climate Change (IPCC) Tier 1 default value of 1% (0.03 –3%) EF for all fertilizers (IPCC, 2014). EFs reported are within a similar range for EFs calculated by Harty *et al.* (2016) in a permanent pasture in Ireland (0.58 - 3.1%), Cowan *et al.* (2020) in managed grasslands across the British Isles (0.7 – 1.3%) and Smith *et al.* (2012) in grassland and arable sites across the United Kingdom (0.9 - 3.93%). While a control treatment was not used in this study, we estimate that EFs with the inclusion of a cumulative control N_2O-N flux (Krol *et al.* 2016) would be 1.25%, 1.09% and 1.16% for EC and CH by the arithmetic and Bayesian methods respectively. Our study suggests that a default EF value for mineral fertilizer is too simplistic to account for the variability of N_2O at different spatial and temporal scales. The Tier 1 approach does not incorporate changes in emissions due to agricultural management or environmental variability (Dobbie and Smith, 2003). When considering the development of national and regional level EFs for N_2O (Tier 2), it is essential that management data (e.g. fertilizer rates) is available over different spatial and temporal scales in order to produce robust estimates of N_2O emissions (Skiba *et al*. 2012).

5. CONCLUSIONS

Fluxes of N_2O measured by CH and EC were most comparable when (1) N_2O fluxes were high (>115 μg N_2O-N m^{-2} hr^{-1}); (2) both methodologies were measuring fluxes over the same space and time; and (3) when the number of CH replicates were ≥ 15 on a given sampling day. Measurements of N_2O emissions using the EC technique were greater than CH flux measurements (arithmetic or Bayesian) 76% of the time over the outlined comparison periods. The Bayesian method was useful in upscaling CH N_2O flux measurements and providing reliable means and confidence intervals by accounting for the log-normally distributed nature of the data. Where the CH sample size was ≥ 15, the arithmetic and the Bayesian method showed similar daily averaged fluxes over the comparison periods. Where n ≤ 5, uncertainties in CH flux measurements calculated by the Bayesian method were large and asymmetrical due to the inability to fit an arithmetic mean from a log-normally distributed data set where the sample size is low. A multi-variate linear model that incorporates environmental data was used to gap-fill annual N_2O fluxes measured by EC and showed a strong correlation with measured flux values (R^2 = 0.92). Annual cumulative N_2O fluxes from January to December 2019 from gap-filled EC fluxes and CH fluxes derived from the arithmetic and Bayesian method, were 3.35 (± 0.5) kg N ha^{-1}, 2.98 (± 0.17) kg N $ha^{-1}$and 3.13 (± 0.24) kg N ha^{-1} respectively. EFs from EC and

CH by the arithmetic and Bayesian method were 1.46%, 1.30% and 1.36%, respectively. N_2O emissions were greatest following CAN fertilizer application when conditions for denitrification were favourable (WFPS > 60%). In order lower EFs from mineral N fertilizer application, applications should be made where conditions for denitrification are limited, such as low soil moisture content and rainfall. Where potential hotspots of N_2O are present on agricultural landscapes (Cowan *et al.* 2017), N fertilizer application should be avoided on theses hotspot areas or nitrification and urease inhibitors should be used to reduce the availability of N for N_2O production (Luo *et al.* 2016)

Declaration of competing interest

The authors declare that they have no known competing financial interests or personal relationships that could have appeared to influence the work reported in this paper.

Acknowledgements

The authors gratefully acknowledge A. Lawless for facilitating the research on the Johnstown Castle Dairy Farm and G. Gillen for gas chromatography analysis. This research was financially supported under the National Development Plan, through the Research Stimulus Fund, administered by the Department of Agriculture, Food and the Marine, Manipulation and Integration of Nitrogen Emissions (MINE) grant number 15S655.

References

Askew, E.F. (2012) 'Inorganic non-metallic constituents; Method 4500-NO3- H. Automated hydrazine reduction method.' In Rice. E.W. et al. (eds) *Standard Methods for the Examination of Waters and Waste-Water*. 22nd Edition. USA: American Public Health Association, 4-128

Bain, W. G. Hutyra, L. Patterson, D.C. Bright, A.V. Daube, B.C. Munger, J.W. Wofsy. S.C. (2005) Wind-induced error in the measurement of soil respiration using closed dynamic chambers. *Agricultural and Forest Meteorology*, **131**, 225-32

Bell, M. Cloy, J. Topp, C. Ball, B. Bagnall, A. Rees, R. Chadwick, D. (2016). Quantifying N_2O emissions from intensive grassland production: The role of synthetic fertilizer type, application rate, timing and nitrification inhibitors. *The Journal of Agricultural Science,* **154(5),** 812-827

Bertora, C. Matteo P. Simone P. Carlo G. Dario S. (2018) Assessment of Methane and Nitrous Oxide Fluxes from Paddy Field by Means of Static Closed Chambers Maintaining Plants Within Headspace. *Journal of visualized experiments: JoVE*: 56754.

Burba, G. (2013) *Eddy covariance method for method for scientific, industrial, agricultural and regulatory applications*. USA: LI-COR Biosciences

Butterbach-Bahl K, Baggs E.M. Dannenmann, M. Kiese, R. Zechmeister-Boltenstern S. (2013) Nitrous oxide emissions from soils: how well do we understand the processes and their controls. *Philosophical Transactions of the Royal Society B,* **368**, 20130122.doi:10.1098/rstb.2013.0122

Butterbach-Bahl, K. Dannenmann, M. (2011) Denitrification and associated soil N_2O emissions due to agricultural activities in a changing climate. *Current Opinion in Environmental Sustainability* , **3**, 389–395

Cai, T. Flanagan, L.B. Syed, K.H. (2010), Warmer and drier conditions stimulate respiration more than photosynthesis in a boreal peatland ecosystem: Analysis of automatic chambers and eddy covariance measurements. *Plant, Cell & Environment*, **33**, 394-407.

Chadwick, D.R. Cardenas, L. Misselbrook, T.H. Smith, K.A. Rees, R.M. Watson, C.J. McGeouh, K.L. Williams, J.R. Cloy, J.M. Thorman, R.E. Dhanoa, M.S. (2014) Optimizing chamber methods for measuring nitrous oxide emissions from plot-based agricultural experiments. *European Journal of Soil Science,* **65**, 295-307.

Choudhary, M. A. Akramkhanov, A. Saggar, S. (2002) Nitrous oxide emissions from a New Zealand cropped soil: tillage effects, spatial and seasonal variability. *Agriculture, Ecosystems and Environment*, **93**, 33–43

Christensen, S. Ambus, P. Arah, J. R. Clayton, H. Galle, B. Griffith, D. W. T. Hargreaves, K. J. Klemedtsson, L. Lind, A.-M. Maag, M. Scott, A. Skiba, U. Smith, K. A. Welling, M. Wienhold, F. G (1996) Nitrous oxide emissions from an agricultural field: comparison between measurements by flux chamber and micrometeorological techniques. *Atmospheric Environment*, **30**, 4183–4190

Clough, T. J. Rochette, P. Thomas, S.M. Pihlatie, M. Christiansen, J.R. Thorman, R.E. (2020) Global Research Alliance N_2O chamber methodology guidelines: Design considerations, *Journal of Environmental Quality*, **49**, 1081-91.

Cowan, N.J. Levy, P.E. Famulari, D. Anderson, M. Reay, Skiba, D.S. (2017) Nitrous oxide emission sources from a mixed livestock farm. *Agriculture, Ecosystems and the Environment,* **243**, 92-102

Cowan, N. Levy, P. Drewer, J. Carswell, A. Shaw, R. Simmons, I. Bache, C. Marinheiro, J. Brichet, J. Sanchez-rodriguez, A.R. Cotton, J. Hill, P.W. Chadwick, D.R. Jones, D.L. Misselbrook, T.H. Skiba, U. (2019) Application of Bayesian statistics to estimate nitrous oxide emission factors of three nitrogen fertilisers on UK grasslands. *Environment International*, **128**, 362–370

Cowan, N. Levy, P. Maire, J. Coyle, M. Leeson, S.R. Famulari, D. Carozzi, M. Nemitz, E. Skiba, U. (2020) An evaluation of four years of nitrous oxide fluxes after application of ammonium nitrate and urea fertilizers measured using the eddy covariance method. *Agricultural and Forest Meteorology*, **280**, 107812. https://doi.org/10.1016/j.agrformet.2019.107812

Davidson, E.A. Keller, M. Erickson, H.E. Verchot, L.V. Veldkamp, E. (2000) Testing a conceptual model of soil emissions of nitrous and nitric oxides. *Bioscience*, **50**, 667.

Davidson, E. A. Savage, K. Verchot, L.V. Navarro, R. (2002) Minimizing artifacts and biases in chamber-based measurements of soil respiration, *Agricultural and Forest Meteorology*, **113**, 21-37.

Environmental Systems Research Institute (ESRI) (2011) ArcGIS Desktop: Release 10. Redlands, CA: Environmental Systems Research Institute

De Klein, C.A.M. Harvey, M.J. Clough, T. Rochette, P. Kelliher, F. Venetera, R. Alfaro,M. Chadwick, D. (2015) *Nitrous Oxide Chamber Methodology Guidelines*. Edition 1.1. Wellington: Ministry of Primary Industries (MPI)

Dobbie, K.E. Smith, K.A. (2003) Impact of different forms of N fertilizer on N_2O emissions from intensive grassland. *Nutrient, Cycling and Agroecosystems*. **67,** 37–46.

Dorich, C. Conant, R, Grace, P. R. Barton, L. de Rosa, D. Wagner-Riddle, C. Fehr, B. (2020). Global Research Alliance N_2O emissions in an upland cropping system of the humid tropics. *Communications in Soil Science and Plan Analysis*, **38**, 189–204.

Fageria, N.K. V.C. Baligar. (2005) Enhancing nitrogen use efficiency in crop plants. *Advances in Agronomy*, **88**, 97–185

Felber, R. Münger, A. Neftel, A. Ammann, C. (2015) Eddy covariance methane flux measurements over a grazed pasture: effect of cows as moving point sources. *Biogeosciences*, **12**, 3925–3940

Finkelstein,P.L. Sims, P.F. (2011) Sampling error in eddy correlation flux measurements. *Journal of Geophysical Research*, **106**, 3503–9

Foken, T. (2003) Angewandte Meteorologie, Mikrometeorologische Methoden. Heidelberg: Springer

Fratini, G. Ibrom, A. Arriga, N. Burba, G. Papale, D. (2012) Relative humidity effects on water vapour fluxes measured with closed-path eddy-covariance systems with short sampling lines. *Agricultural and Forest Meteorology*, **165**, 53–63

Fuchs, K. Hortnagl L, Buchmann, N. Eugster, W. Snow, V. Merbold, L. (2018) Management matters: testing a mitigation strategy for nitrous oxide emissions using legumes on intensively managed grassland. *Biogeosciences* , **15**, 5519-5543.

Groffman, P.M. Butterbach-Bahl, K. Fulweiler, A.J.G. Morse, J.L. Stander, E.K. Tague, C. Tonitto, C. Vidon, P. (2009) Challenges to incorporating spatially and temporally explicit phenomena (hotspots and hot moments) in denitrification models. *Biogeochemistry*, **93,** 49-77

Hargreaves, P. Bob, R. Horgan, G. Ball. B. (2015). Size and Persistence of Nitrous Oxide Hot-Spots in Grazed and Ungrazed Grassland. *Environment and Natural Resources Research.* **5.** 10.5539/enrr.v5n4p1.

Harty, M.A. Forrestal, P.J. Watson, C.J. McGeough, K.L. Carolan, R. Elliot, C. Krol, D. Laughlin, R.J. Richards, K.G. Lanigan, G.J. (2016). Reducing nitrous oxide emissions by changing N fertilizer use from calcium ammonium nitrate (CAN) to urea based formulations. *Science of the Total Environment,* **563–564**: 576–586.

Hyde, B. Forrestal, P.Jahangir, M.M.R. Ryan, M. Fanning, A.F. Carton, O. Lanigan, G. Richards, K. (2016). The interactive effects of fertilizer nitrogen with dung and urine on nitrous oxide emissions in grassland. *Irish Journal of Agricultural and Food Research*. **55**. 1-9

Intergovernmental Panel on Climate Change (IPCC) (2013) "Anthropogenic and natural radiative forcing" In: Myhre, G. et al. (eds) *Climate Change 2013: The Physical Science Basis. Contribution of Working Group I to the Fifth Assessment Report of the Intergovernmental Panel on Climate Change*. Cambridge University Press: Cambridge UK and New York, NY, USA, 659–740

Intergovernmental Panel on Climate Change (IPCC), (2014) "Climate Change 2014: Synthesis Report. Contribution of Working Groups I, II and III to the Fifth Assessment Report of the Intergovernmental Panel on Climate Change " In : R.K. Pachauri and L.A. Meyer (eds.) . IPCC: Switzerland, 151

Jones, S. K. Famulari, D. Di Marco, C. F. Nemitz, E. Skiba, U. M. Rees, R. M. Sutton, M. A. (2011) Nitrous oxide emissions from managed grassland: a comparison of eddy covariance and static chamber measurements. *Atmospheric Measurement Techniques*, **4**, 2179– 2194,

Jones, D.I. Willett, V.B. (2006) Experimental evaluation of methods to quantify dissolved organic nitrogen (DON) and dissolved organic carbon (DOC) in soil. *Soil Biology and Biochemistry*, **38**, 991-999

Kaimal, J.C. Finnigan, J.J. (1994) *Atmospheric Boundary Layer Flows.* Oxford University Press: Oxford

Kljun, N. Calanca, P. Rotach, M.W. Schmid, H.P. (2015) A simple two-dimensional parameterisation for Flux Footprint Prediction (FFP). *Geoscientific Model Development*, **8**, 3695-3713,

Kormann, R. Meixner. F.X. (2001) An analytical footprint model for nonneutral stratification. *Boundary-Layer Meteorology*, **99**,207–224.

D.J. Krol. Carolan, R. Minet. E. McGeough, K.L. Watson, V. Forrestal, P.J. Lanigan, G.J. Richards, K.G (2016) Improving and disaggregating N_2O emission factors for ruminant excreta on temperate pasture soils. *Science of the Total Environment*, 568, 327-338

Krol, D.J. Carolan, R. Minet, E. McGeough, K.L. Watson, C.J. Forrestal, P.J. Lanigan, G.J. Richards, K.G. (2017) Improving and disaggregating N_2O emission factors for ruminant excreta on 13 temperate pasture soils. *Science of The Total Environment*, **568**, 327-338.

Kroon, P.S. Hensen, A. van den Bulk, W.C.M. Jongejan, P.A.C. Vermeulen, A.T. (2008) The importance of reducing the systematic error due to non-linearity in N2O flux measurements by static chambers. Nutrient Cycling in Agroecosystems, **82**,175–186

Lammirato, C. Lebender, U. Tierling, J. Lammel, J. (2018) Analysis of uncertainty for N_2O fluxes measured with the closed-chamber method under field conditions: Calculation method, detection limit, and spatial variability. *Journal of Plant Nutrition and Soil Science*, **181**, 78–89.

Laville, P. Henault, C. Renault, P. Cellier, P. Oriol, A. Devis, X. Flura, D. Germon, J. C. (1997) Field comparison of nitrous oxide emission measurements using micrometeorological and chamber methods. *Agronomie*, **17**, 375–388

Levy, P. Cowan, N. van Oijen, M. Famulari, D. Drewer, J. Skiba, U. (2017) Estimation of cumulative fluxes of nitrous oxide: uncertainty in temporal upscaling and emission factors: Estimation of cumulative fluxes of nitrous oxide. *European Journal of Soil Science*, **68**, 400-411

Liáng, L.L. Campbell, D.I. Wall, A.M. Schipper, L.A. (2018) Nitrous oxide fluxes determined by continuous eddy covariance measurements from intensively grazed pastures: temporal patterns and environmental controls. *Agriculture, Ecosystem and Environment*, **268**, 171–180

Linn, D.M and Doran, J.W. (1984) Effect of Water-Filled Pore Space on Carbon Dioxide and Nitrous Oxide Production in Tilled and Non-Tilled Soils. *Soil Science Society of America Journal,* **48**, 1267-1272

Lognoul, M. Debacq, A. De Ligne, A. Dumont, B. Manise, T. Bodson, B. Heinesch, B. Aubinet, M. (2019) N_2O flux short-term response to temperature and topsoil disturbance in a fertilized crop: An eddy covariance campaign*. Agricultural and Forest Meteorology,* **271***,* 193-206

Luo, J. van der Weerden, T. Thomas, S. de Klein, C. Lindsey, S. Judge, A. (2016) 'Hotspot Areas of Nitrous Oxide Emissions from Pasture Grazed by Dairy Cows', Agresearch (published online ahead of print May 2016). Available at: https://www.mpi.govt.nz/dmsdocument/28296/direct (Accessed 15th February 2021)

Luo, J. Wyatt, J. van der Weerden, T.J.Thomas, S.M. de Klein, C.A.M. Yan, L. Rollo, M. Lindsey, S. Ledgard, S.F. Li, J. Ding, W. Qin, S. Zhang, N. Bolan, N. Kirkham, M.B. Bai, Z. Ma, L. Zhang, X. Wang, H. Liu, H. Rys, G. (2017) Potential Hotspot Areas of Nitrous Oxide Emissions From Grazed Pastoral Dairy Farm Systems. *Advances in Agronomy,* **145**, 205-268

Maire, J. Krol, D. Pasquier, D. Cowan, N. Skiba, U. Rees, R.M. Reay, D. Lanigan, G.J. Richards, K.G. (2020) Nitrogen fertilizer interactions with urine deposit affect nitrous oxide emissions from grazed grasslands. *Agriculture, Ecosystems and Environment*, **290**, 106784,

Mauder, M. Foken, T. (2011) Documentation and Instruction Manual of the Eddy Covariance Software Package TK2. Arbeitsergebnisse, Universit¨at Bayreuth, Abteilung Mikrometeorologie, ISSN 1614-8916 46.

McClain, M. E. Elizabeth W. Boyer, C. Dent, L. Gergel, S.E. Grimm, N.B. Groffman, P.M. Hart, S.C. Harvey, J.W. Johnston, C.A. Mayorga, E. McDowell, W.H. Pinay, G. (2003) Biogeochemical Hot Spots and Hot Moments at the Interface of Terrestrial and Aquatic Ecosystems. *Ecosystems,* **6**, 301-12.

Merbold, L. Decock, C. Eugster, W. Fuchs, K. Wolf, B. Buchmann, N. Hörtnag, L. (2020) Memory effects on greenhouse gas emissions (CO_2, N_2O and CH_4) following grassland restoration? *Biogeosciences Discussions*, https://doi.org/10.5194/bg-2020-141

Mishurov, M. Kiely, G. (2011) Gap filling techniques for the annual sums of nitrous oxide fluxes. *Agricultural and Forest Meterology,* **151**, 1763-17676.

Moffat, A.M. Papale, D. Reichstein, M. Hollinger, D.Y. Richardson, A.D. Barr, A.G. Beckstein, C. Braswell, B.H. Churkina, G. Desai, A.R. Falge, E. Gove, J.H. Heimann, M. Hui, D. Jarvis, A.J. Kattge, J. Noormets, A. Stauch, V.J. (2007) Comprehensive comparison of gap-filling techniques for eddy covariance net carbon fluxes. *Agricultural and Forest Meteorology,* **147**, 209–232.

Moncrieff, J. B. Clement R. Finnigan, J. Meyers, T. (2004) *Averaging, detrending and filtering of eddy covariance time series, in Handbook of micrometeorology: a guide for surface flux measurements*, eds. Lee, X., W. J. Massman and B. E. Law. Dordrecht: Kluwer Academic, 7-31

Nashina, K. Takenaka, C. Ishizuka, S. (2009) Spatiotemporal variation in N_2O flux within a slope in a Japanese cedar (Cryptomeria japonica) forest. *Biogeochemistry*, **96**, 163-175

Pickett S.T.A. White P.S. (1985) *The ecology of natural disturbance and patch dynamics*. USA: Academic

Pihlatie, M. Rinne, J. Ambus, P. Pilegaard, K. Dorsey, J. R. Rannik, U. Markkanen, T. Launiainen, S. Vesala, T. (2005)Nitrous oxide emissions from a beech forest floor measured by eddy covariance and soil enclosure techniques. *Biogeosciences*, **2**, 377-387

Plummer, M. (2015) JAGS: A Program for Analysis of Bayesian Graphical Models Using Gibbs Sampling. URL http://citeseer.ist.psu.edu/plummer03jags.html.

Rafique, R. Hennessy, D. Kiely, G. (2011) Nitrous Oxide Emission from Grazed Grassland Under Different Management Systems. *Ecosystems*, **14,** 563-582

Rochette, P. Hutchinson, G.L. (2005) 'Measurement of Soil Respiration in situ: Chamber Techniques.' in, *Micrometeorology in Agricultural Systems*.

Rochette, P. (2011) Towards a standard non-steady-state chamber methodology for measuring soil N_2O emissions. *Animal Feed Science and Technology*.,**166**, 141–146.

RStudio Team (2020). RStudio: Integrated Development for R. RStudio, PBC, Boston, URL http://www.rstudio.com/.

Scherbak, I. Robertson, G.P. (2019) Nitrous Oxide (N_2O) Emissions from Subsurface Soils of Agricultural Ecosystems. *Ecosystems*, **22**, 1650-1663

Schrier-Uijl, A. P. Kroon, P. S. Hensen, A. Leffelaar, P. A. Berendse, F. Veenendaal, E. M. (2010) Comparison of chamber and eddy covariance-based CO_2 and CH_4 emission estimates in a heterogeneous grass ecosystem on peat. *Agricultural and Forest Meteorology*, **150**, 825-831

Shurpali, N.J. Rannik, Ü. Jokinen, S. Lind, S. Biasi, C. Mammarella, I. Peltola, O. Pihlatie, M. Hyvönen, N, Räty, M. Haapanala, S. Zahniser, M. Virkajärvi, P. Vesala, T. Martikainen, P.J. Reay, D.S. Saikawa, E. Cameron, K.C. Di, H.J. Moir, J.L. Rees, R.M. Bouwman, A.F. Boumans, L.J.M. Batjes, N.H. Chadwick, D.R. Kutzbach, L. Maljanen, M. Livingston, G. Hutchinson, G. Matson, P.A. Harris, R.C. Pattey, E. Baldocchi, D. Nicolini, G. Castaldi, S. Fratini, G. Valentini, R. Pihlatie, M.K. Savage, K. Phillips, R. Davidson, E. Werle, P. Rannik, Ü. Butterbach-Bahl, K. Baggs, E.M, Dannenmann, M. Kiese, R. Zechmeister-Boltenstern, S. Wrage, N. Groenigen, J.Wv. Oenema, O. Baggs, E.M. Braker, G. Conrad, R. Philippot, L. Kool, D.M. Spott, O. Russow, R. Stange, C.F. Laughlin, R.J. Stevens, R.J. Müller, C. Laughlin, R.J. Spott, O. Rütting, T. Stange, C.F. Cleemput, O. Samater, A.H. Wallenstein, M.D. Myrold, D.D. Firestone, M. Voytek, M. Tiedje, J.M. Zehnder, A.J.B. Mosier, A.R. Morgan, J.A. King, J.Y. LeCain, D. Milchunas, D.G. Kowalchuk, G.A. Stephen, J.R. Tamura, Y. Moriyama, M. Kusel, K. Drake, H.L. Denmead, O. Ryden, J.C. Lund, L.J. Focht, D.D. Blackmer, A.M. Robbins, S.G. Bremner, J.M. Christensen, S. Ostrom, N.E. Neftel, A. Zona, D. Groenigen, J.Wv. Murray, P.J. Hughes, M. Donnelly, C. Crozier, A. Wheeler, C.T. Tavi, N.M. Denef, K. Macduff, J.H. Bakken, A.K. Grosso, S.J.Del. Inselsbacher, E. Zhang, J. Müller, C. Cai, Z. Inselsbacher, E. Näsholm, T. Werdin-Pfisterer, N.R. Kielland, K. Boone, R.D. Inselsbacher, E. Oyewole, O.A. Näsholm, T. (2016) Neglecting diurnal variations leads to uncertainties in terrestrial nitrous oxide emissions. *Scientific Reports*, **6**, 25739-25739.

Skiba, U. Jones, S.K. Dragosits, U. Drewer, J. Fowler, D. Rees, R.M. Pappa, V.A. Cardenas, L. Chadwick, D. Yamulki, S. Manning, A.J. (2012) UK emissions of the greenhouse gas nitrous oxide. Philosophical Transactions of the Royal Society B: *Biological Sciences* **367**, 1175–1185

Smith, K.A. Dobbie, K.E. Thorman, R. Watson, C.J. Chadwick, D.R. Yamulki, S. Ball, B.C. (2012) The effect of N fertilizer forms on nitrous oxide emissions from UK arable land and grassland. *Nutrient, Cycling and Agroecosystems*, **93,** 127–149. http://dx.doi.org/10.1007/s10705-012-9505-1.

Soussana, J.F. Tallec, T. Blanfort, V. (2010) Mitigating the greenhouse gas balance of ruminant production systems through carbon sequestration in grasslands. *Animal,* **4**, 334–350

Standing Committee of Analysts (1981) "Ammonia in waters 1981(Methods for the Examination of Water and Associated Materials)". UK,: HMSO

Tan, I. Vanes, H. Duxbury, J. Melkonian, J. Schindelbeck, R. Geohring, L. Hively, W. Moebius, B. (2009) Single-event nitrous oxide losses under maize production as affected by soil type, tillage, rotation, and fertilization. *Soil and Tillage Research*, **102**, 19–26

Thompson, K. Bent, E. Abalos, D. Wagner-Riddle, C. Dunfield, K. (2016) Soil microbial communities as potential regulators of in situ N_2O fluxes in annual and perennial cropping systems. *Soil Biology and Biochemistry*, **103**, 262-273.

Vickers, D. Mahrt, L. (1997) Quality control and flux sampling problems for tower and aircraft data. *Journal of Atmospheric and Oceanic Technology*, **14**, 512–526

Voglmeier, K. Six, J. Jocher, M. Ammann, C. (2019) Grazing-related nitrous oxide emissions: from patch scale to field scale. *Biogeosciences,* **16**, 1685–1703.

Waldo, S. Russell, E. S. Kostyanovsky, K., Pressley, S. N., O'Keeffe, P. T. Huggins, D. R. Stöckle, O.C. Pan, W.I. Lamb, B.K. (2019) N_2O emissions from two agroecosystems: High spatial variability and long pulses observed using static chambers and the flux-gradient technique. *Journal of Geophysical Research: Biogeosciences*, **124**, 1887–1904

Wang, K. Liu, C. Zheng, X. Pihlatie, M. Li, B. Haapanala, S. Vesala , T. Liu, H. Wang, L. Liu, G. Hu, F. (2013a) Comparison between eddy covariance and automatic chamber techniques for measuring net ecosystem exchange of carbon dioxide in cotton and wheat fields. *Biogeosciences*, **10**, 6865-6877

Wecking, A.R. Walla, A.R. Liang, L.L. Lindsey, S.B. Luoc, J. Campbell, D.I. Schipper, L.A. (2020) Reconciling annual nitrous oxide emissions of an intensively grazed dairy pasture determined by eddy covariance and emission factors. *Agriculture, Ecosystems and Environment,* **287**, 106646

Wild, P. Hordan, R. Leplay, A. Vincent, R. (1996) Confidence intervals for probabilities of exceeding threshold limits with censored log-normal data. *Environmetrics,* **7**, 247–259.

World Meteorological Organisation (WMO) (2019) WMO GREENHOUSE GAS BULLETIN The State of Greenhouse Gases in the Atmosphere Based on Global Observations through 2018. Retrieved from: https://library.wmo.int/doc_num.php?explnum_id=10100 on 29/01/20.

Zanatta, J. A., Bayer, C. Vieira, F. C.B. Gomes, J. Tomazi, M. (2010). Nitrous oxide and methane fluxes in south Brazilian gleysol as affected by nitrogen fertilizers. *Revista Brasileira de Ciência do Solo*, **34,** 1653-1665.

APPENDICES

Table A.1: Chamber (CH) flux measurements (N_2O-N μg m^{-2} hr^{-1}) derived from the arithmetic and Bayesian method where FP refers to CH measurements inside the footprint of the eddy covariance footprint.

	Arithmetic Method						Bayesian Method					
		95% C.I.			95% C.I.			95% C.I.			95% C.I.	
Date	mean	lwr	upr	mean	lwr	upr	mean	lwr	upr	mean	lwr	upr
		CH_{All}			CH_{FP}			CH_{Bayes}			$CH_{Bayes-FP}$	
8/1/2019	2.67	1.69	3.66	2.82	1.87	3.77	2.69	1.63	3.81	2.84	1.72	3.98
17/1/2019	1.82	1.1	2.53	1.24	0.31	2.17	1.83	1.05	2.64	1.26	0.16	2.42
25/1/2019	3.04	2.09	3.99	3.07	1.68	4.46	3.05	2.02	4.15	3.14	1.25	5.26
1/2/2019	1.52	0.64	2.4	1.16	-0.39	2.72	1.54	0.55	2.55	1.3	-1.02	4.12
7/2/2019	1.97	1.06	2.88	2.38	1.42	3.35	1.98	1	3.01	2.42	1.12	3.89
4/3/2019	1.89	0.64	3.14	4.14	0.59	7.68	1.91	0.66	3.23	4.71	-0.25	11.47
5/3/2019	1.9	0.11	3.69	0.31	-1.19	1.81	1.95	0.24	3.79	0.37	-1.39	2.24
6/3/2019	538.89	359.79	717.99	626.7	490.93	762.47	677.88	400.25	1223.65	670.86	491.66	985.96
7/3/2019	356.28	178.38	534.17	234.11	30.5	437.72	391.46	232.66	701.46	949.89	113.9	25944.48
8/3/2019	165.66	99.28	232.05	147.1	44.64	249.57	202.68	111.35	380.34	318.16	74.1	1211.42
11/3/2019	74.75	44.07	105.43	28.68	-5.46	62.83	80.56	49.22	130.54	33.95	9.53	86.26
12/3/2019	36.27	18.05	54.49	10.77	1.81	19.72	36.8	22.14	57	11.54	3.73	22.31
14/3/2019	7.37	1.86	12.88	1.48	-7.84	10.79	8.06	2.33	15.41	14.76	-7.93	61.6
19/3/2019	7.43	3.99	10.87	2.71	1.75	3.67	7.46	4.59	10.72	2.73	1.6	3.9
26/3/2019	5.62	2.65	8.58	1.93	0.78	3.08	5.65	3.15	8.44	1.98	0.25	3.83
1/4/2019	5.67	1.45	9.89	1.9	-2.45	6.25	5.65	2.45	9.17	3.34	-4.12	15.66
2/4/2019	33.99	15.39	52.6	3.2	2.04	4.36	33.89	20.27	52.36	3.43	0.54	7.24
3/4/2019	18.05	2.97	33.13	-0.2	-1.95	1.54	17.19	8.49	28.67	0.1	-3.8	5.28
4/4/2019	26.19	-0.54	52.92	5.29	-4.55	15.13	22.37	11.82	36.93	9.75	-3.59	36.72
5/4/2019	117.92	53.07	182.77	63.54	0.22	126.87	134.64	70.71	258.17	171.12	24.86	634.1
8/4/2019	79.57	38.65	120.5	26.73	14.52	38.93	81	48.97	132.2	30.3	14.73	58.3
10/4/2019	89.67	46.23	133.12	67.51	1.81	133.22	93.08	56.52	153.62	424.98	24.85	6218.68
11/4/2019	77.84	46.81	108.87	39.48	25.05	53.91	82.2	52.83	127.82	46.14	23.14	89.87
16/4/2019	36.46	19.27	53.65	8.44	4.62	12.27	36.77	23.67	55.03	19.06	2.06	25.26
17/4/2019	16.64	5.06	28.23	8	-9.42	25.41	17.25	8.02	29.85	211.1	-7.43	2405.36
23/4/2019	44.68	13.62	75.74	13.02	5.11	20.94	41.93	23.26	70.38	21.11	2.51	54.37
24/4/2019	20.5	-10.03	51.04	7.01	3.24	10.77	14.67	5.68	26.74	50.58	0.43	34.83
4/6/2019	24.06	14.05	34.07	24.13	14.8	33.46	24.25	16.35	34.25	25.22	15.69	37.79
5/6/2019	18.98	9.56	28.39	10.78	5.53	16.04	18.91	11.87	27.58	12.08	3.52	25.71
6/6/2019	39.63	25.55	53.7	52.76	32.52	73	39.86	28.98	53.88	56.81	35.46	92.08
7/6/2019	15.51	12.07	18.95	18.35	10.46	26.23	15.64	12.28	19.38	19.52	10.51	32.31
8/6/2019	16.49	11.32	21.65	16.92	9.07	24.77	16.64	12.11	21.82	20.53	7.97	39.2
10/6/2019	11.5	9.16	13.85	12.84	9.11	16.56	11.57	9.27	14.09	13.11	8.67	18.27
11/6/2019	8.28	5.82	10.74				8.32	6.1	10.73			
12/6/2019	23.02	15.62	30.43	25.66	12.62	38.71	23.29	16.76	31.02	28.95	13.46	55.17
13/6/2019	22.69	14.67	30.71	21.59	13.49	29.68	22.83	16.52	30.36	22.86	13.44	36.8
17/6/2019	101.03	60.55	141.51	126.67	33.92	219.42	106.14	69.37	164.17	203.53	64.29	620.08
19/6/2019	27.83	18.74	36.92	26.4	5.4	47.4	28.09	20.56	37.16	80.44	8.31	198.83
26/6/2019	12.95	9.79	16.12	21.14	12.41	29.87	13.06	10.02	16.37	23.2	11.75	40.66
27/6/2019	8.56	6.47	10.66	13.95	9.42	18.48	8.62	6.53	10.85	14.57	8.3	22.28
7/8/2019	6.81	3.17	10.44	8.29	-1.22	17.79	7.07	3.24	11.5	13.56	-0.93	37.75
9/8/2019	38.64	14.63	62.64	17.86	6.92	28.79	37.52	23	58.43	20.49	7.73	42.6
13/8/2019	10.96	8.15	13.76	13.56	8.34	18.78	11.01	8.43	13.78	14.01	8.6	20.84
21/8/2019	3.86	2.18	5.54	6.68	0.7	12.66	3.88	2.27	5.56	7.96	0.15	19.91
28/8/2019	1.52	-0.24	3.28	1.28	-3.01	5.58	1.6	-0.23	3.58	1.8	-3.12	8.28
2/9/2019	4.12	2.15	6.09	5.37	1.51	9.23	4.16	2.25	6.27	5.83	0.79	12.43
10/9/2019	14.73	11.09	18.37	14.46	9.19	19.73	14.82	11.34	18.65	14.76	9.78	20.69
12/9/2019	11.44	8.11	14.76	12.13	4.34	19.93	11.6	8.3	15.3	13.26	4.65	25.31
13/9/2019	18.55	14.06	23.03	18.01	7.13	28.9	18.78	14.39	23.73	19.79	8.52	36.58
14/9/2019	1.23	-2.73	5.19	5.22	-4.24	14.67	1.4	-2.15	5.51	6.95	-2.77	22.43
16/9/2019	7.69	4.47	10.91	7.91	3.37	12.45	7.79	4.79	11.19	8.41	3.28	14.95
17/9/2019	17.86	13.71	22	18.61	10.2	27.01	18.03	14.16	22.44	19.49	11.36	30.5
19/9/2019	2.12	-0.9	5.13	-0.42	-6.24	5.41	2.47	-1.07	6.59	1.15	-6.59	13.64
20/9/2019	3.28	0.4	6.17	7.51	-0.91	15.93	3.43	0.54	6.63	9.98	-1.26	30.24
24/9/2019	417.14	221.24	613.04	255.44	147.27	363.61	438.86	279.03	727.07	349.62	167.12	843.77
25/9/2019	127.98	82.16	173.8	84.9	48.31	121.5	131.64	93.19	189.39	92.51	56.63	155.62
1/10/2019	66.95	38.75	95.15	95.42	24.7	166.13	67.24	46.49	96.73	282.22	46.41	1265.31
2/10/2019	67.99	34.56	101.43	94.83	8.46	181.2	71.35	41.91	118.69	510.06	37.71	6100.45
10/10/2019	26.55	10.76	42.34	24.03	7.06	41.01	26.37	15.16	41.41	26.62	11.79	51.1
16/10/2019	15.14	10.43	19.84	19.95	7.42	32.49	15.27	11.07	20.1	22.53	9.23	45.23
22/10/2019	14.07	4.6	23.54				13.75	7.59	21.25			
31/10/2019	5.72	2.31	9.12	10.14	1.88	18.4	5.94	2.44	9.94	11.77	2.14	26.52
4/11/2019	7.65	3.41	11.89	12.54	-8.55	33.64	7.71	4.28	11.71	53.89	-2.67	161.41
14/11/2019	2.5	1.09	3.91	4.04	1.35	6.72	2.53	1.15	4	4.38	0.4	9.38
20/11/2019	9.95	6.46	13.45	14.3	6.36	22.25	10.07	6.9	13.75	15.23	7.2	26.51
27/11/2019	-0.4	-4.19	3.38	-2.62	-13.34	8.09	-0.01	-3.96	4.81	2.68	-11.32	35.51
3/12/2019	5.83	1.86	9.8	15.67	0.99	30.35	5.79	2.77	9.11	19.79	4.02	50.31

11/12/2019	18.85	8.28	29.41	26.16	-1.32	53.64	18.89	10.83	29.17	52.29	7.29	138

Table A.2: Eddy covariance (EC) flux measurements (N_2O-N μg m^{-2} hr^{-1}) where EC_{CH} are EC flux measurements made during the time of chamber measurements

			95% C.I.			95% C.I.
Date	mean	lwr	upr	mean	lwr	upr
			EC_{All}		E_{CH}	
8/1/2019	16.4	10.38	23.67	4.82	3.92	5.46
17/1/2019	39.22	20.32	59.34	9.12	5.51	12.72
25/1/2019	13.44	4.52	20.01			
1/2/2019						
7/2/2019	4.1	-33.88	17.44	2.03	0.53	4.59
4/3/2019	25.1	5.89	53.12	7.2	1.75	9.82
5/3/2019	25	5.31	116.41	4.18	1.67	10.73
6/3/2019	537.74	162.79	1021.16	168.7	160.6	177.36
7/3/2019	218.07	115.45	441.38	71.14	71.14	71.14
8/3/2019	48.03	22.47	76.69	19.56	17.1	22.48
11/3/2019	10.06	-17.68	28.79	4.16	0.55	6.45
12/3/2019	9.92	-7.72	30.55			
14/3/2019	9.72	-5.9	27.45			
19/3/2019	9.99	-14.34	28.85	3.49	0.9	6.33
26/3/2019	9.68	1.39	26.98	2.52	2.52	2.52
1/4/2019	21.05	2.53	86.79			
2/4/2019	61.17	26.91	93.3	14.56	12.91	17.57
3/4/2019	25.41	11.96	55.64			
4/4/2019	98.95	88.17	110.28			
5/4/2019	180.98	70.84	278.95	60.62	45.7	82.95
8/4/2019	307.41	234.05	344.38			
10/4/2019	133.34	98.68	168.46			
11/4/2019	101.08	56.79	136.32	27.66	24.47	31.96
16/4/2019	57.3	32.11	79.06	13.93	12.23	16.39
17/4/2019	39.83	28.1	57.91	10.47	8.61	12.54
23/4/2019	41.08	-19.44	126.04	26.37	20.4	34.53
24/4/2019	46.91	25.19	86.82	13.74	7.15	24.45
4/6/2019	40.54	-1.02	103.26	15.06	13	17.12
5/6/2019	40.36	12.9	71.04	8.77	4.48	17.45
6/6/2019	65.89	12.66	178.47	14.98	4.3	22.05
7/6/2019	138.33	57.21	269.42	24.13	21.82	30.59
8/6/2019	219.31	83.01	325.55	53.5	46.33	60.43
10/6/2019	63.42	63.42	63.42	17.62	17.62	17.62
11/6/2019	81.14	20.24	148.9	27.91	19.83	35.99
12/6/2019	21.41	-42	90.34	1.42	-9.83	6.78
13/6/2019						
17/6/2019	51.12	-0.36	94.35	13.16	11.17	17.72
19/6/2019	237.28	142.7	412.34	71.93	49.83	90.86
26/6/2019	63.74	29.74	96.32	16.8	8.61	22.32
27/6/2019	14.58	-64	65.86	6.57	-7.36	16.95
7/8/2019	17.14	-60.08	80.02	-9.84	-15.78	-5.93
9/8/2019	19.06	7.73	31.66	8.78	8.18	9.83
13/8/2019						
21/8/2019						
28/8/2019	16.71	6.61	28.21	6.04	4.73	7.73
2/9/2019	19.2	-8.12	50.88	11.11	6.09	14.77
10/9/2019	16.17	-0.91	37.41	7.28	3.82	10.25
12/9/2019	29.92	12.09	49.92	5.14	3.7	9.85
13/9/2019	17.57	6.11	37.25	5.82	1.17	10.44
14/9/2019	19.71	8.43	35.66	4.46	2.96	6.17
16/9/2019	19.99	7.16	35.56	4.96	2.92	8.9
17/9/2019	17.04	9.22	28.97	5.09	3.05	7.98
19/9/2019	13.94	6.11	25.15	2.68	1.49	4.38
20/9/2019	17.92	-13.88	80.08	15.32	5.14	36.02
24/9/2019	315.1	127.22	510.38	90.86	66.6	110.8
25/9/2019	270.17	159.41	354.39	70.02	58.71	80.96
1/10/2019	90.16	53.72	135.19			
2/10/2019	82.88	52.05	111.01	21.31	18.01	24.6
10/10/2019	32.1	12.74	59.02	9.61	6.78	11.37
16/10/2019	17.08	5.21	28.5	4.55	3.77	4.95
22/10/2019						
31/10/2019	11.26	-21.39	27.59			
4/11/2019	13.59	-2.36	40.82			
14/11/2019	-1.21	-1.21	-1.21			
20/11/2019	10.39	-7.97	21.21	5.11	4.3	5.92
27/11/2019	15.39	5.76	30.62			

3/12/2019	-3.14	-42.78	20.88	-3.26	-12.75	5.5
11/12/2019	26.27	9.83	45.88	7.17	6.76	8.01

Table A.3: The full output from a regression subset model explaining the variance in log(N_2O-N) fluxes by water-filled pore space (WFPS%), rainfall (mm) air temperature (Tair ^{o}C) and soil temperature (Tsoil ^{o}C) over rolling averages of 6 hrs^{-1}, 12 hrs^{-1}, 24 hrs^{-1}, 48hrs^{-1} and 100 hrs^{-1} periods in the 30 days following fertilizer application (Fertilizer) and in the 30 days outside of fertilizer applications (Background).

Variable	Treatment	R^2
WFPS 48 hr^{-1}	Fertilizer	0.50
WFPS 100 hr^{-1}	Fertilizer	0.50
WFPS 6 hr^{-1}	Fertilizer	0.50
Rainfall 100 hr^{-1}	Fertilizer	0.50
Rainfall 48 hr^{-1}	Fertilizer	0.50
Rainfall 24 hr^{-1}	Fertilizer	0.49
Rainfall 12 hr^{-1}	Fertilizer	0.49
Rainfall 6 hr^{-1}	Fertilizer	0.49
Tsoil 100 hr^{-1}	Fertilizer	0.48
Tair 100 hr^{-1}	Fertilizer	0.43
Tair 48 hr^{-1}	Fertilizer	0.40
WFPS 100 hr^{-1}	Background	0.31
Rainfall 48 hr^{-1}	Background	0.31
Rainfall 24 hr^{-1}	Background	0.31
Tsoil 48 hr^{-1}	Background	0.30
Tsoil 12 hr^{-1}	Background	0.29
Tair 100 hr^{-1}	Background	0.27

Table A.4: Output from a linear multivariate model for log(N_2O-N) emissions measured by eddy covariance 30 days post fertilizer application (Fertilizer) and 30 days outside of the fertilizer application (Background) using rolling averages of air (Tair) and soil temperature (Tsoil), water filled pore space (WFPS %) and rolling sums of rainfall over 6 hrs^{-1}, 12 hrs^{-1}, 24 hrs^{-1}, 48 hrs^{-1} and 100 hrs^{-1} periods

Treatment	Parameter	Estimate	Standard Error	t Value
Fertilizer	Intercept	-1.99	0.51	-3.91
	Tair 48 hr^{-1}	0.24	0.02	10.96
	(Tair 48 hr^{-1}) ^2	-0.01	0.00	-7.22
	Tair 100 hr^{-1}	-0.85	0.04	-23.21
	(Tair 100 hr^{-1}) ^2	0.03	0.00	19.96
	Tsoil 100 hr^{-1}	0.68	0.03	25.86
	(Tsoil 100 hr^{-1}) ^2	-0.02	0.00	-23.81
	(Rainfall 6 hr^{-1}) ^2	0.00	0.00	-8.04
	Rainfall 12 hr^{-1}	-0.03	0.00	-5.27
	(Rainfall 12 hr^{-1}) ^2	0.00	0.00	7.80
	Rainfall 24 hr^{-1}	0.02	0.00	5.35
	(Rainfall 24 hr^{-1}) ^2	0.00	0.00	2.12
	(Rainfall 48 hr^{-1}) ^2	0.00	0.00	-12.95
	Rainfall 100 hr^{-1}	0.00	0.00	22.62
	WFPS 6 hr^{-1}	0.11	0.02	6.91
	(WFPS 6 hr^{-1}) ^ 2	0.00	0.00	-6.08
	WFPS 48 hr^{-1}	0.29	0.03	9.48
	(WFPS 48 hr^{-1}) ^2	0.00	0.00	-8.68
	WFPS 100 hr^{-1}	-0.18	0.03	-5.60
	(WFPS 100 hr^{-1}) ^2	0.00	0.00	3.61
	Days Since Fertilizer App. 24 hr^{-1}	-0.01	0.00	-6.70
	(Days Since Fertilizer App. 24 hr^{-1}) ^2	0.00	0.00	4.07
Background	Intercept	4.04	0.27	14.71
	Tair 100 hr^{-1}	-0.05	0.02	-2.99
	(Tair 100 hr^{-1}) ^2	0.01	0.00	7.25
	(Tsoil 12 hr^{-1}) ^2	0.00	0.00	11.50
	Tsoil 48 hr^{-1}	0.05	0.01	4.12
	(Tsoil 48hr^{-1}) ^2	-0.01	0.00	-11.64
	Rainfall 24 hr^{-1}	0.02	0.00	6.42
	(Rainfall 24 hr^{-1}) ^2	0.00	0.00	-4.54
	Rainfall 48 hr^{-1}	-0.01	0.00	-8.91
	WFPS 6 hr^{-1}	0.15	0.01	10.71
	(WFPS 6 hr^{-1}) ^ 2	0.00	0.00	-9.33
	WFPS 48 hr^{-1}	-0.13	0.02	-8.30
	(WFPS 48 hr^{-1}) ^ 2	0.00	0.00	11.68
	(WFPS 100 hr^{-1}) ^ 2	0.00	0.00	-20.99
	Days Since Fertilizer App. 100hr^{-1}	0.00	0.00	-5.01
	(Days Since Fertilizer App. 100 hr^{-1}) ^ 2	0.00	0.00	3.37

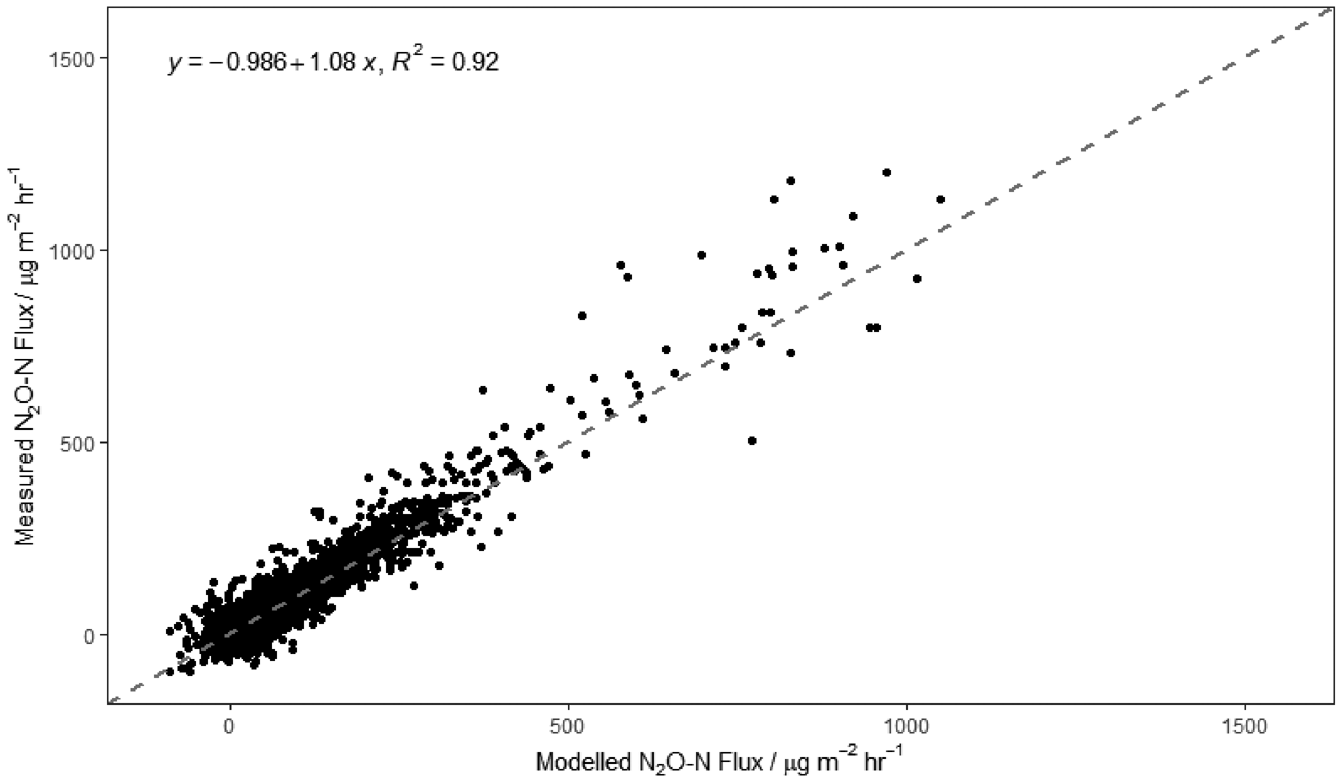

Figure A.1: The correlation between measured and linearly modelled N_2O-N flux values where the broken line represents the 1:1 ratio.

Table A.5: Cumulative N_2O fluxes from mean daily chamber and half-hourly eddy covariance (EC) flux measurements from seven comparison periods (see Table 3 for dates) where EC_{All} is all measured EC measurements over the comparison period, EC_{CH} is measured EC measurements during the time of chamber measurements, CH_{All} and CH_{Bayes} are all chamber flux measurements daily averaged using the arithmetic and the Bayesian mean, respectively and CH_{FP} and $CH_{Bayes-FP}$ are daily averaged chamber flux measurements within the footprint of the EC tower using the arithmetic mean and the Bayesian mean, respectively.

Comparison #	EC_{All}				EC_{CH}				CH_{All}				CH_{FP}				$CH_{Bayes-All}$				$CH_{Bayes-FP}$			
	N		95% C.I.		*N*		95% C.I.		*N*		95% C.I.		*N*		95% C.I.		*N*		95% C.I.		*N*		95% C.I.	
		mean	upr	lwr		mean	upr	lwr		mean	upr	lwr		mean	upr	lwr		mean	upr	lwr		mean	upr	lwr
	N_2O-N kg^{-1} ha^{-1} comparison^{-1}																							
1	94	0.127	0.090	-0.085	12	0.026	0.019	-0.018	105	0.016	0.009	-0.009	43	0.015	0.009	-0.008	105	0.017	0.009	-0.009	43	0.016	0.009	-0.009
2	367	0.257	0.178	-0.168	31	0.079	0.055	-0.054	295	0.366	0.247	-0.221	87	0.303	0.218	-0.200	295	0.430	0.296	-0.261	87	0.582	0.423	-0.351
3	341	0.483	0.265	-0.224	39	0.107	0.048	-0.046	353	0.295	0.141	-0.127	59	0.127	0.059	-0.056	353	0.305	0.148	-0.132	59	0.511	0.217	-0.174
4	321	0.444	0.215	-0.192	43	0.119	0.053	-0.051	390	0.172	0.067	-0.063	94	0.199	0.075	-0.069	390	0.176	0.068	-0.064	94	0.319	0.110	-0.095
5	99	0.064	0.022	-0.021	14	0.025	0.009	-0.008	150	0.054	0.032	-0.031	39	0.049	0.026	-0.025	150	0.054	0.032	-0.031	39	0.056	0.030	-0.029
6	339	0.579	0.180	-0.134	58	0.150	0.050	-0.047	388	0.473	0.157	-0.122	123	0.375	0.119	-0.101	388	0.491	0.163	-0.126	123	0.699	0.192	-0.134
7	283	0.153	0.084	-0.082	34	0.029	0.019	-0.019	299	0.141	0.083	-0.081	69	0.166	0.084	-0.081	299	0.142	0.083	-0.082	69	0.290	0.138	-0.129

1020